



Article

Identification and Preclinical Development of a 2,5,6-Trisubstituted Fluorinated Pyridine Derivative as a Radioligand for the Positron Emission Tomography Imaging of Cannabinoid Type 2 Receptors

Ahmed Haider, Luca C. Gobbi, Julian Kretz, Christoph Ullmer, Andreas Brink, Michael Honer, Thomas J. Woltering, Dieter Muri, Hans Iding, Markus Bürkler, Martin Binder, Christian Bartelmus, Irene Knuesel, Pal Pacher, Adrienne Müller Herde, Francesco Spinelli, Hazem Ahmed, Kenneth Atz, Claudia Keller, Markus Weber, Roger Schibli, Linjing Mu, Uwe Grether, and Simon Mensah Ametamey
J. Med. Chem., **Just Accepted Manuscript** • DOI: 10.1021/acs.jmedchem.0c00778 • Publication Date (Web): 11 Aug 2020

Downloaded from pubs.acs.org on August 17, 2020

Just Accepted

“Just Accepted” manuscripts have been peer-reviewed and accepted for publication. They are posted online prior to technical editing, formatting for publication and author proofing. The American Chemical Society provides “Just Accepted” as a service to the research community to expedite the dissemination of scientific material as soon as possible after acceptance. “Just Accepted” manuscripts appear in full in PDF format accompanied by an HTML abstract. “Just Accepted” manuscripts have been fully peer reviewed, but should not be considered the official version of record. They are citable by the Digital Object Identifier (DOI®). “Just Accepted” is an optional service offered to authors. Therefore, the “Just Accepted” Web site may not include all articles that will be published in the journal. After a manuscript is technically edited and formatted, it will be removed from the “Just Accepted” Web site and published as an ASAP article. Note that technical editing may introduce minor changes to the manuscript text and/or graphics which could affect content, and all legal disclaimers and ethical guidelines that apply to the journal pertain. ACS cannot be held responsible for errors or consequences arising from the use of information contained in these “Just Accepted” manuscripts.

Identification and Preclinical Development of a 2,5,6-Trisubstituted Fluorinated Pyridine Derivative as a Radioligand for the Positron Emission Tomography Imaging of Cannabinoid Type 2 Receptors

Ahmed Haider¹, Luca Gobbi², Julian Kretz², Christoph Ullmer², Andreas Brink², Michael Honer², Thomas J. Woltering², Dieter Muri², Hans Iding³, Markus Bürkler², Martin Binder², Christian Bartelmus², Irene Knuesel², Pal Pacher⁴, Adrienne Müller Herde¹, Francesco Spinelli¹, Hazem Ahmed¹, Kenneth Atz², Claudia Keller¹, Markus Weber⁵, Roger Schibli^{1,6}, Linjing Mu^{1,6}, Uwe Grether², Simon M. Ametamey^{1*}

¹Institute of Pharmaceutical Sciences, ETH Zurich, Vladimir-Prelog-Weg 4, 8093 Zurich, Switzerland

²Pharma Research and Early Development, Roche Innovation Center Basel, F. Hoffmann-La Roche, 4070 Basel, Switzerland

³Pharma Technical Development, F. Hoffmann-La Roche Ltd., 4070 Basel, Switzerland

⁴Laboratory of Cardiovascular Physiology and Tissue Injury, National Institute of Health/NIAAA, 5625 Fishers Lane, Rockville, Maryland 20852, USA

⁵Neuromuscular Diseases Unit/ALS Clinic, Kantonsspital St. Gallen, 9007 St. Gallen, Switzerland

⁶Department of Nuclear Medicine, University Hospital Zurich, 8091 Zurich, Switzerland

Abstract

Despite the broad implications of the cannabinoid type 2 receptor (CB2) in neuroinflammatory processes, a suitable CB2-targeted probe is currently lacking in clinical routine. In this work, we synthesized 15 fluorinated pyridine derivatives and tested their binding affinities towards CB2 and CB1. With a subnanomolar affinity (K_i for CB2) of 0.8 nM and a remarkable selectivity factor of $> 12'000$ over CB1, RoSMA-18-d₆ exhibited outstanding *in vitro* performance characteristics and was radiofluorinated with an average radiochemical yield of $10.6 \pm 3.8\%$ ($n = 16$) and molar activities ranging from 52 - 65 GBq/ μ mol (radiochemical purity $> 99\%$). [¹⁸F]RoSMA-18-d₆ showed exceptional CB2 attributes as demonstrated by *in vitro* autoradiography, *ex vivo* biodistribution and positron emission tomography (PET). Further, [¹⁸F]RoSMA-18-d₆ was used to detect CB2 upregulation on post-mortem human ALS spinal cord tissues. Overall, these results suggest that [¹⁸F]RoSMA-18-d₆ is a promising CB2 PET radioligand for clinical translation.

Introduction

Although the effects of cannabis sativa were known for centuries, the main pharmacologically active component, Δ^9 -tetrahydrocannabinol (THC), was first isolated and characterized in 1964¹. Notably, the isolation of THC has prompted calls for extensive structure activity-relationship studies, ultimately leading to the discovery of the cannabinoid receptors type 1 (CB1) and type 2 (CB2) in the early nineties^{2,3}. Characterized by seven transmembrane domains, CB1 and CB2 belong to the rhodopsin-family of G-protein coupled receptors (GPCRs) that mainly transduce extracellular signals *via* inhibition of adenylyl cyclase (AC), thereby suppressing the cyclic adenosine monophosphate (cAMP) pathway⁴. Given the complexity of cannabinoid downstream signaling and the various interactions with other signaling pathways, it is not surprising that cannabinoid receptor activation may result in diverse cellular responses such as cell migration, proliferation, survival and apoptosis⁵⁻⁷. Initial drug discovery activities focused on the development of non-subtype selective agonists, however, their use was plagued by severe psychotropic adverse events including memory loss, altered locomotor activity and impaired cognition⁸⁻¹⁰. These adverse events were primarily attributed to the high abundance of CB1 in the central nervous system (CNS)¹¹. The identification of CB2 as a key player in (neuro)inflammatory processes along with its relatively low abundance in the healthy mammalian CNS have channeled the development of CB2-selective ligands^{12,13}. Particularly, CB2-targeted agonists were anticipated to exert pharmacological effects while being well tolerated¹⁴⁻¹⁷. Further, CB2-selective positron emission tomography (PET) imaging probes may allow the subclinical diagnosis of inflammatory conditions, thereby enabling precision medicine¹⁸. Notwithstanding the diversity of CB2-targeted probes in preclinical development, no suitable CB2 PET radioligand is available in current clinical practice. Although the previously reported CB2 PET radioligand [¹¹C]NE40 has been tested in healthy volunteers and Alzheimer's Disease (AD) patients, it was not possible to detect CB2 upregulation with [¹¹C]NE40 in AD patients, conceivably owing to off-target binding to CB1^{19,20}. Other reported CB2 PET radioligands were deemed unsuitable due to inappropriate pharmacokinetics, the presence of radiometabolites in the brain and high lipophilicity as well as non-specific binding²¹⁻²⁸.

As part of our efforts to develop a suitable CB2 PET radioligand, we recently reported on a pyridine-based probe, [¹⁸F]**3** (**Figure 1**), that exhibited a CB2 affinity of 6 nM and a selectivity factor of nearly 700 over CB1²⁹. In spite of the single digit nanomolar CB2 affinity, [¹⁸F]**3** displayed poor *in vivo* specificity and a fast washout from CB2-rich rat spleen²⁹. To overcome the shortcomings of [¹⁸F]**3**, and based on knowledge gained from our previous study, we designed and synthesized 15 new derivatives of [¹⁸F]**3**, which were obtained by structural modifications at position 6 of the pyridine core. These structure activity-relationship (SAR) studies led to the identification of [¹⁸F]RoSMA-18-d₆ (**Figure 1**). This new compound exhibited an 8-fold improved CB2 binding affinity of 0.8 nM compared to [¹⁸F]**3** and a remarkable selectivity factor of > 12'000 over CB1. Preclinical evaluation of [¹⁸F]RoSMA-18-d₆ revealed a substantially improved CB2 specificity *in vivo* and a strikingly prolonged tracer retention in the CB2-rich rat spleen, underlining the outstanding performance characteristics of this new radioligand for CB2-targeted *in vivo* imaging.

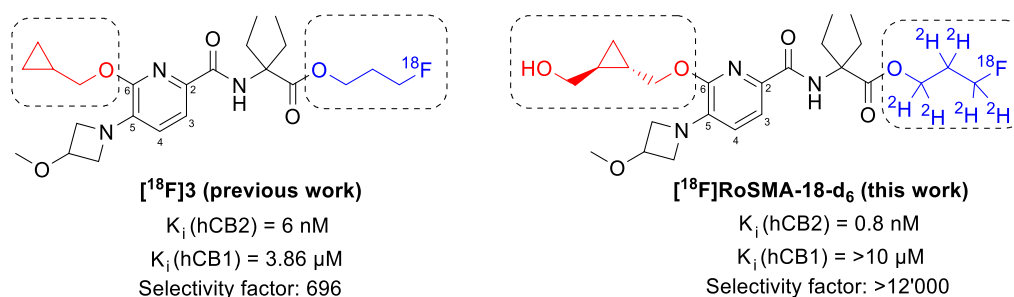


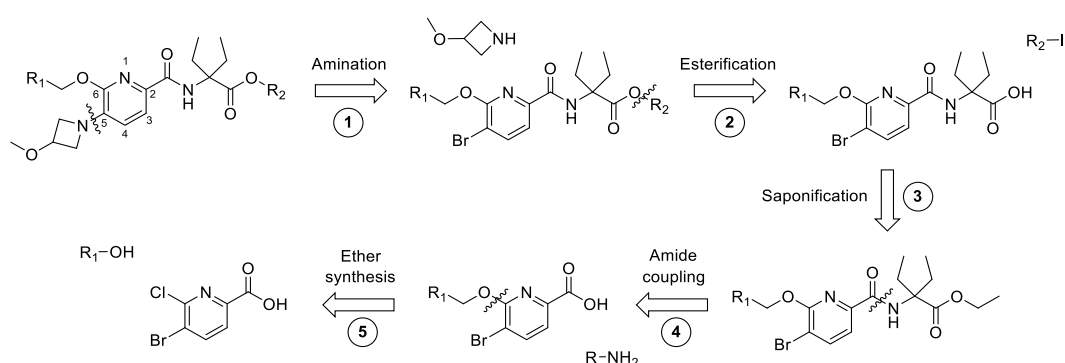
Figure 1: Structures of [¹⁸F]**3** (previous work) and [¹⁸F]RoSMA-18-d₆ (this work) with sites of modification indicated in boxes at positions 2 (blue) and 6 (red).

Results

Structure-activity relationship (SAR)

Structural modifications of lead compound **3** were performed according to the simplified retrosynthetic analysis depicted in **Scheme 1**. While methoxy-azetidine was introduced by Pd-catalyzed cross-coupling to a bromo-pyridine precursor (retrosynthetic step 1), ester formation was accomplished *via* the reaction of free carboxylic acids with the respective alkyl halides (retrosynthetic step 2). Carboxylic acids were obtained by saponification of the respective ethyl esters (retrosynthetic step 3). Importantly,

the ethoxy moiety served as a protection group during amide formation that was typically achieved with an activated ester using the coupling reagent TBTU (retrosynthetic step 4). Concurrently, the use of an ethoxy protection group during amide formation obviated the necessity for retrosynthetic steps 2 and 3 for target compounds (**1-8** and **15**, **Table 1**) bearing an ethyl ester functionality. Alkyl fluoride groups were introduced either by transforming an OH functionality into a sulfonate leaving group, followed by nucleophilic substitution with fluoride or by direct treatment of the carboxylic acids with commercially available fluorinated alkylating reagents.



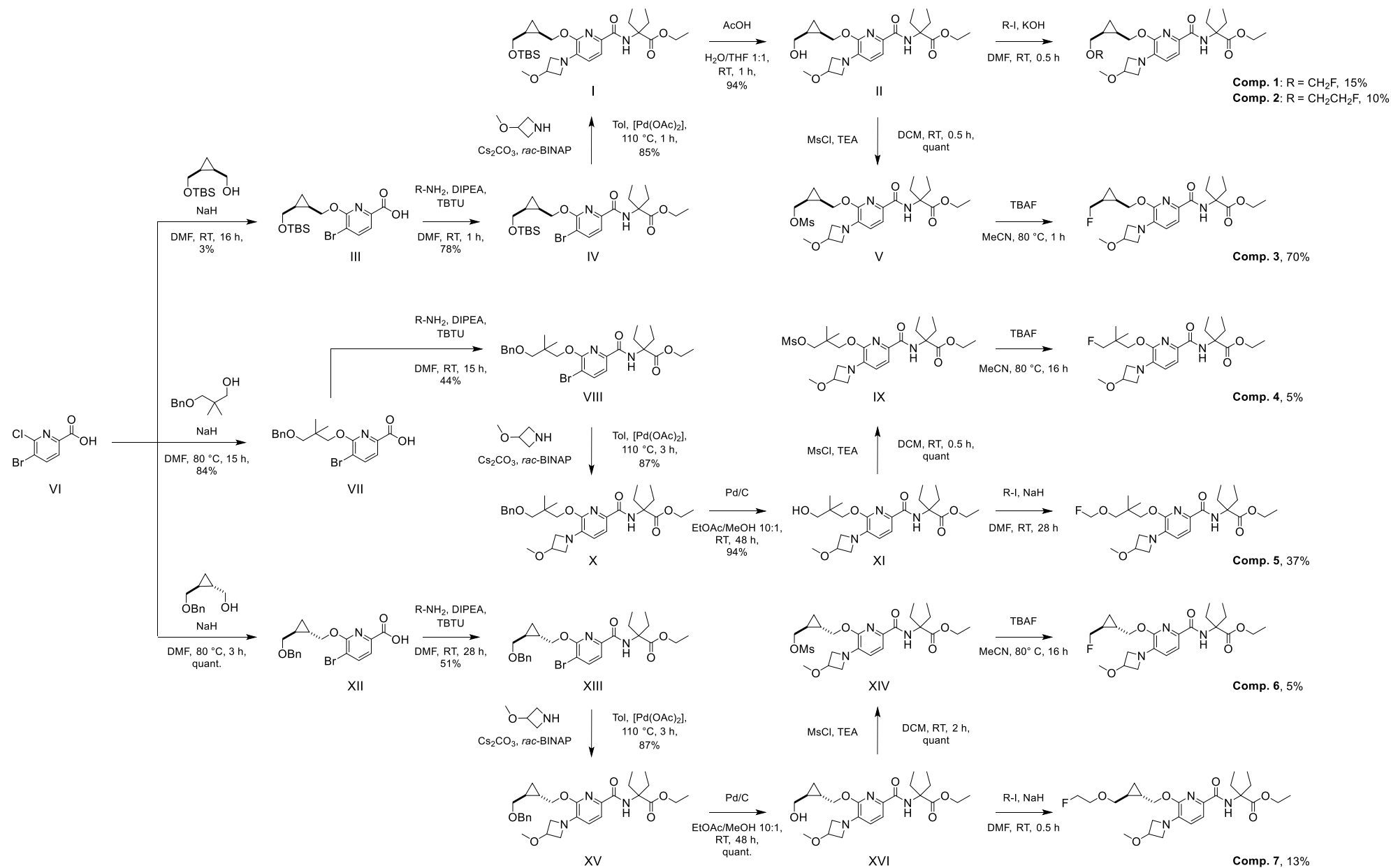
Scheme 1: General retrosynthetic scheme for the design of 2,5,6-trisubstituted pyridines depicted in **Table 1**.

From previous studies, we have established that a 3-methoxy-azetidine substituent at position 5, along with an amide at position 2 of the pyridine core were key features that led to high CB2 binding affinities for this class of compounds²⁹. Additionally, the adjacent diethyl moiety was important for CB2 affinity and selectivity over CB1. The ester functionality was well tolerated and allowed fast derivatization of the alkoxy side chain²⁹. Accordingly, the main focus of the present SAR study was to screen different substituents at position 6 of the pyridine core in combination with either an ethoxy- or fluoroalkoxy side chain at the ester functionality. One important aspect for compound design was the introduction of a fluorine atom in one of these two positions to allow for ¹⁸F-labeling.

Cis and *trans* isomers (racemic, relative stereochemistry) of disubstituted cyclopropanes were envisioned for substituents at position 6 of the pyridine core. Accordingly, disubstituted cyclopropanes were prepared from commercially available diethyl *cis*-cyclopropane-1,2-dicarboxylate and diethyl *trans*-cyclopropane-1,2-dicarboxylate, respectively (**Supplemental Figure 1**).

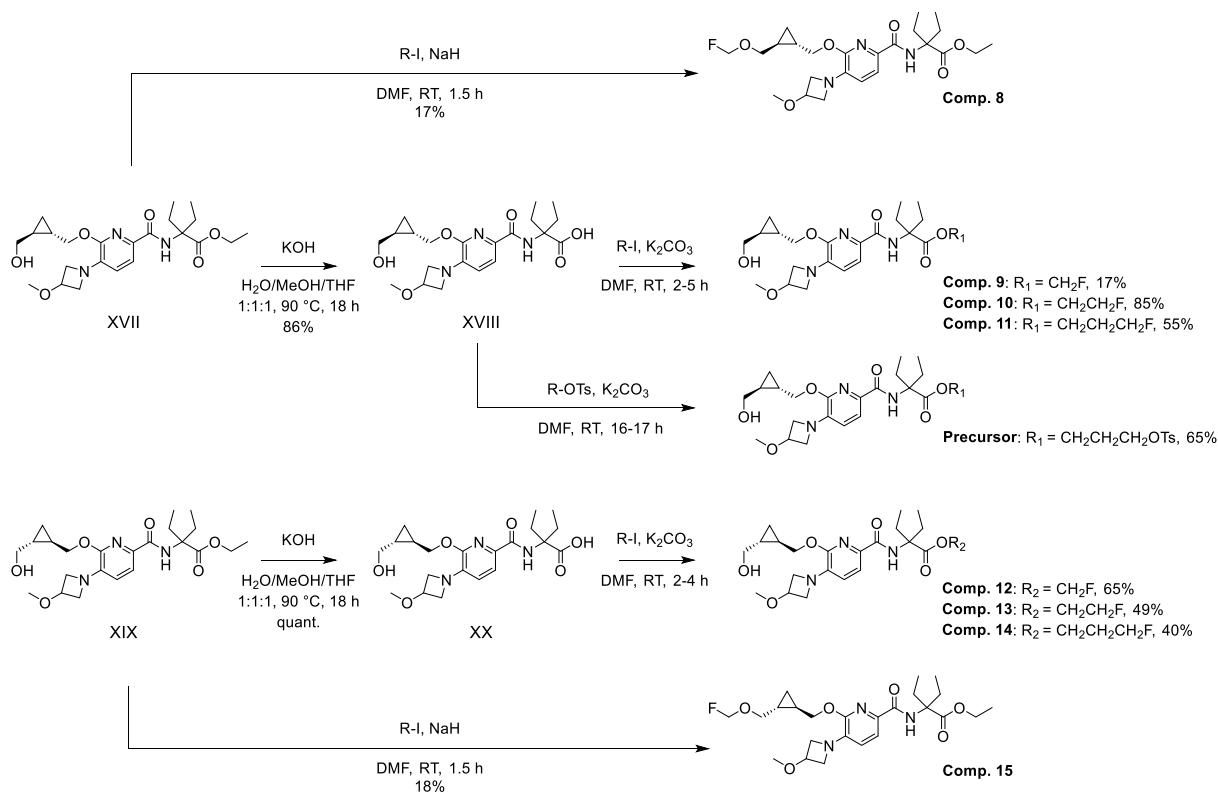
Starting from picolinic acid **VI**, target compounds **1-7** were synthesized either in five steps (compounds **1**, **2**, **5** and **7**) or in six steps (compounds **3**, **4** and **6**) as shown in **Scheme 2**. Initially, ethers **III**, **VII** and

1
2
3 **XII** were obtained *via* nucleophilic aromatic substitution of the chlorine atom in **VI** with the appropriate
4 alcoholate. Subsequent amide couplings were accomplished *via* the activated ester using TBTU as
5 coupling reagent in chemical yields ranging from 44-78%. Buchwald-Hartwig cross-coupling conditions
6 were used to introduce 3-methoxy-azetidine, providing amides **I**, **X** and **XV** in chemical yields of 85%,
7 87% and 87%, respectively. Alcohol deprotections were performed either by treatment of benzyl-
8 bearing intermediates **X** and **XV** with Pd/C or under acidic conditions for the TBS-protected
9 intermediate **I**. Esterification of alcohols **II**, **XI** and **XVI** with fluoromethyl and fluoroethyl iodide,
10 respectively, gave final compounds **1**, **2**, **5** and **7** in chemical yields ranging from 10-37%. Fluorination
11 was carried out *via* the activated mesylate precursors **V**, **IX** and **XIV**, which were synthesized from the
12 respective alcohols in quantitative yields using excess mesyl chloride. Treatment of the mesylate
13 precursors with TBAF afforded target compounds **3**, **4** and **6** in variable yields as depicted in **Scheme**
14 **2**. Enantiopure key intermediates **XVII** and **XIX** were obtained *via* chiral resolution of **XVI** by HPLC
15 and were used for the synthesis of enantiopure target compounds **8-15** (**Scheme 3**). While the synthesis
16 of target structures **8** and **15** was achieved by direct fluoromethylation of the respective alcoholate, target
17 compounds **9-14** were obtained in two steps *via* ethyl ester hydrolysis and subsequent introduction of
18 fluoroalkoxy side chains of variable chain lengths (n = 1-3) as shown in **Scheme 3**. The precursor for
19 radiofluorination was obtained by reacting carboxylic acid **XVIII** with propyl tosylate. Further, a *de*
20 *novo* synthesis of enantiopure precursor was developed *via* the previously reported procedure of
21 diastereoselective cyclopropanation³⁰ (**Supplemental Figures 2 and 3**). The product of this
22 diastereoselective synthesis was used to confirm the absolute configuration of target compounds
23 depicted in **Scheme 3** by comparison of retention times on chiral HPLC and light polarimetry
24 experiments (**Supplemental information**).



Scheme 2: Synthesis of 2,5,6-trisubstituted pyridines **1-7**. Comp. **1-3**, cis/racemic; Comp. **6** and **7**, trans/racemic.

Binding affinities towards hCB2 and selectivities over hCB1 were determined for all final compounds and are summarized in **Table 1**. In order to estimate blood-brain barrier penetration and non-specific binding to brain tissue, $\log D_{7.4}$ and LIMBA $\log D_{BPL}$ values were measured. Initially, we investigated the influence of cyclopropyl functionalization either *via* fluoromethylation or by introduction of fluoroalkoxy groups of variable chain lengths. These modifications afforded derivatives **1-3**, **6-8** and **15** with high CB2 affinities in the range from 0.3-13 nM (**Table 1**). In sharp contrast, replacement of the cyclopropyl substituent with a geminal dimethyl moiety led to a remarkable reduction in potency and selectivity values, as evidenced by target compounds **4** (K_i hCB2 > 10 μ M) and **5** (K_i hCB2 = 143 nM).

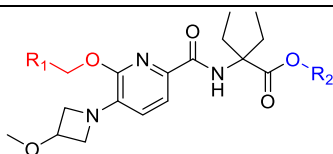


Scheme 3: Synthesis of enantiopure 2,5,6-trisubstituted pyridines **8-15**.

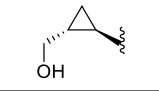
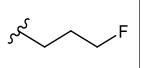
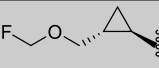
Notably, the stereochemistry of disubstituted cyclopropyl moieties significantly affected the CB2 binding affinity, with *trans*-racemic target compounds **6** and **7** outperforming their *cis*-racemic stereoisomers **3** and **2** (**Table 1**, **6** vs. **3**; K_i hCB2 = 0.3 nM vs. 1 nM and **7** vs. **2**; K_i hCB2 = 4 nM vs. 13 nM). Despite exhibiting the highest CB2 binding affinity, target compound **6** displayed a relatively low selectivity factor of 272 over CB1. Given the high abundance of CB1 in the CNS, this compound was not selected for radiolabeling. Bioisosteric substitution of the fluorine atom with a hydroxyl group

and concurrent introduction of fluoroalkoxy side chains of variable lengths *via* esterification led to a remarkable increase in selectivity over CB1 while retaining the subnanomolar affinity for CB2, as evidenced by the K_i values of derivatives **9**, **10** and **11** (Table 1). Further, the results support the concept that longer fluoroalkoxy side chains favor higher selectivity over CB1. Notably, while the *S,S*-enantiomers **9-11** exhibited subnanomolar CB2 affinities, their respective *R,R*-enantiomers **12-14** displayed a significant reduction in CB2 affinity and selectivity over CB1.

Table 1: Binding affinity (K_i), selectivity index and Lipophilicity ($\log D_{7.4}$ and LIMBA $\log D_{BPL}$) of 2,5,6-trisubstituted pyridines **1-15**.



Cmp.	R ₁	R ₂	$\log D_{7.4}$	LIMBA $\log D_{BPL}$	K_i hCB2 [μ M]	K_i hCB1 [μ M]	K_i CB1/CB2
1			3.42	1.34	0.005	> 10	> 2173
2			4.08	2.23	0.013	2.981	229
3			3.06	2.64	0.001	0.590	675
4			2.45	* n.d.	> 10	> 10	* n.d.
5			* n.d.	* n.d.	0.143	2.437	17
6			3.14	2.46	0.0003	0.094	272
7			4.19	2.04	0.004	2.585	703
8			2.89	<0.1	0.002	0.806	4031
9			3.54	0.93	0.0004	0.547	1503
10			3.60	0.91	0.0003	1.601	5337
11 (RoSMA-18)			3.90	1.70	0.0007	> 10	> 14'286
12			3.49	1.00	0.010	1.622	167
13			3.62	0.91	0.011	3.497	307

14			3.80	1.16	0.019	> 10	> 532
15			3.59	1.88	0.008	1.828	224

* not determined, Comp. **1-3**, cis/racemic; Comp. **6** and **7**, trans/racemic

Overall, the highest CB2 affinities were achieved for hydroxymethylated and fluoromethylated cyclopropyl derivatives as evidenced by the hCB2 K_i -values of compounds **6** (0.3 nM), **10** (0.3 nM), **9** (0.4 nM) and **11** (0.7 nM). Among all the newly designed compounds, **11** exhibited the highest selectivity factor of > 12'000. With this remarkable affinity and selectivity, **11** provided the most appropriate *in vitro* properties for evaluation as a potential CB2 PET radioligand. Hence, this structure was selected for advanced profiling, radiolabeling and biological assessment.

Advanced profiling of target compound **11**

The inhibitory constant (K_i) and half maximal effective concentration (EC_{50}) towards the CB2 receptor were assessed for different species. Competitive binding assays were performed as previously reported²⁹, and revealed single K_i value estimations of 2.0 nM (mouse), 0.7 nM (rat) and 0.1 nM (cynomolgus monkey), respectively, indicating that compound **11** maintains an excellent binding affinity across species. Similarly, functional activity was determined for the CB1 and CB2 receptor using Chinese hamster ovary (CHO) cells stably expressing CB2 in a validated cAMP assay²⁹. Compound **11** was found to be a potent inverse agonist for human CB2 as well as for rodent CB2 (data not shown), while exhibiting virtually no activity on human CB1. To identify potential off-targets, compound **11** was screened at high concentration (1 μ M) against a customized panel of representative proteins as previously described³¹, and was found to be highly selective for the CB2 receptor (selectivity screening included the following targets: CB1, adrenergic receptors α_1 , α_{2A} , β_1 , β_2 , adenosine A_1 and A_3 receptor, angiotensin II receptor type 1, GABA_A receptor, cholecystokinin A receptor, Dopamine receptor D₁, glycine receptor, muscarinic acetylcholine receptors M₁ and M₂, μ - and κ -opioid receptor, PCP receptor, serotonin 1A receptor, diltiazem-inducible calcium channel, monoamine oxidase A, xanthine oxidase, HIV-1 protease, norepinephrine transporter, acetylcholinesterase, 5-HT_{2A/B} and 5-HT₃ receptor, serotonin transporter, glucocorticoid receptor, gelatinase B, peroxisome proliferator-activated

1
2
3 receptor γ , zeta-chain-associated protein kinase 70, prostaglandin F receptor, glycogen synthase kinase-
4
5 3 α and β , cyclin-dependent kinase 2, nicotinic acetylcholine receptors, tyrosine-protein kinase ABL1,
6
7 angiotensin-converting enzyme, phosphodiesterase 3 and 4D2, estrogen receptor α and cyclooxygenase
8
9 2). In spite of its ester group, inverse agonist **11** is chemically stable in aqueous buffers at different pH
10
11 values (1, 4, 6.5, 8, 10) over a period of 2 h at 37 °C showing only slight decomposition at pH 1 (%
12
13 recovery after 2 h at pH: 1, 87%; 4, no degradation detected; 6.5, no degradation detected; 8, 97%; 10,
14
15 93%). The molecule is highly soluble (high throughput solubility = 86 $\mu\text{g/mL}$) and even more
16
17 importantly is capable of efficiently permeating through membranes as illustrated by a high PAMPA
18
19 permeation coefficient P_{eff} of $5.02 \text{ cm/s} \times 10^{-6}$ (55.3% donor / 32.3% membrane / 12.2% acceptor
20
21 compartment) and favorable P-glycoprotein (P-gp) assay data (Papp 217 nm/sec). In the mouse P-gp
22
23 assay compound **11** exhibits an efflux ratio of 4.6, which suggests together with its high permeability
24
25 that crossing the blood brain barrier (BBB) in rodents is feasible. In humans, the P-gp efflux ratio is only
26
27 2.7, therefore it is expected that PET tracer candidate **11** would efficiently cross the BBB in humans.
28
29 An efflux ratio < 4 is considered favorable for brain penetration. In summary, PET tracer candidate **11**
30
31 possesses all physicochemical and pharmacological characteristics that allow for radiolabelling and
32
33 assessment *in vivo*.
34
35
36
37

38 Docking Studies

39
40
41 In order to assess potential interactions within the active site of the CB2 receptor, inverse agonist **11**
42
43 was docked into the CB2 receptor pocket, based on the X-ray structure of inactive state CB2 receptor
44
45 with antagonist AM10257 (PDB: 5ZTY)³². The docking pose illustrates an excellent fit of the ligand
46
47 within the binding cavity and is supported by detailed structure-activity relationship information. In
48
49 addition to the previously reported pyridine-based PET radioligand [¹⁸F]**3**²⁹ the extra primary hydroxyl
50
51 group in position 2 undergoes a critical hydrogen bond interaction with Thr114 (**Figure 2**) which might
52
53 contribute to the subnanomolar binding affinity of target compound **11**.
54
55
56
57
58
59
60

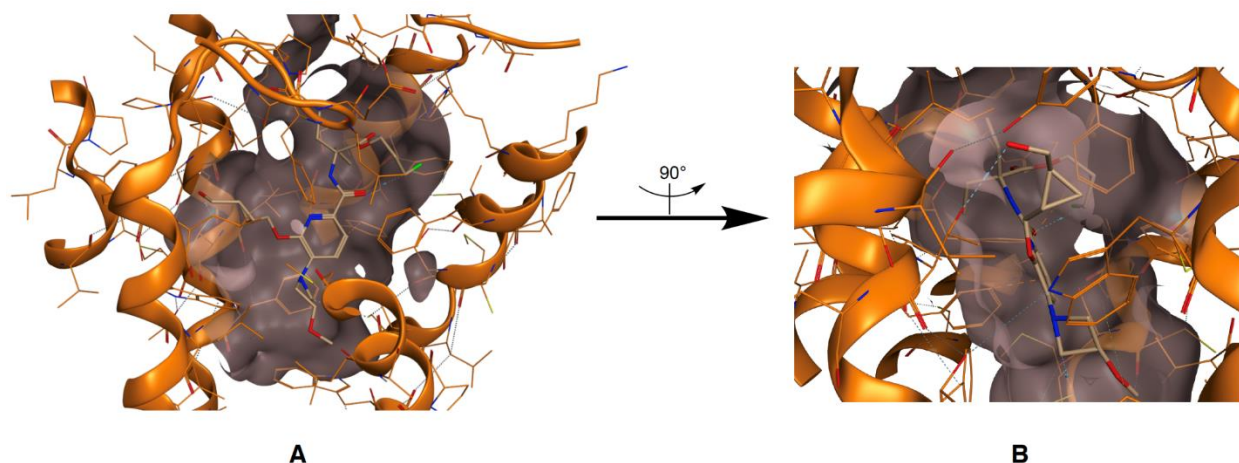
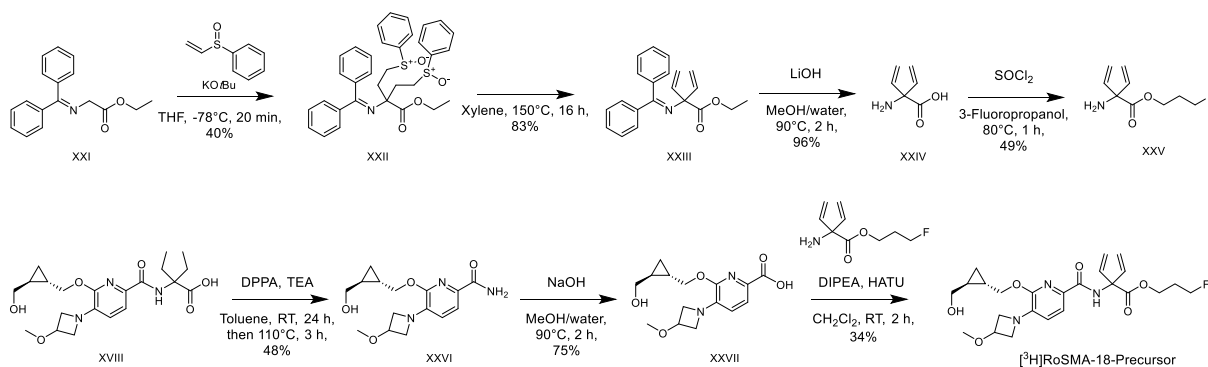


Figure 2: CB2 inverse agonist **11** docked into the binding cavity of inactive state CB2 X-ray structure (PDB: 5ZTY). **A.** Front view, showing binding pose of docked compound **11**. **B.** Side view, highlighting the (1*S*,2*S*)-hydroxy-cyclopropyl configuration, which allows for critical hydrogen bond interaction with the hydroxy group of Thr14. In the foreground single “toggle switch,” Trp6.48 (W258^{6,48}) (orange sticks) is depicted.

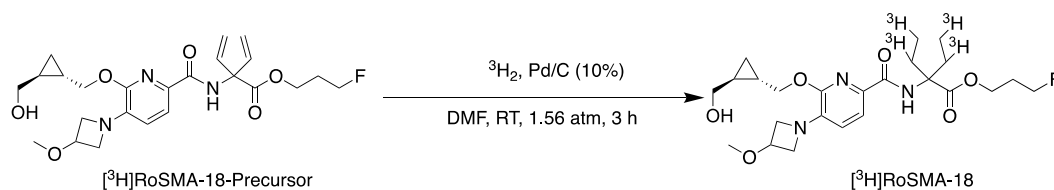
Tritium-Labeling of Compound **11**

Encouraged by the outstanding *in vitro* profile and docking findings of **11**, and with the aim to assess the performance characteristics of tritium-labeled [³H]**11**, codenamed [³H]RoSMA-18, by *in vitro* autoradiography experiments, compound **11** was radiolabeled with tritium after condensing bis-vinyl amino ester **XXV** and picolinic acid **XXVII**. The bis-vinyl group was inserted over two steps starting from diphenylmethyleneglycine ethyl ester **XXI**. Two phenyl sulfoxide ethylene groups were introduced *via* double Michael-Addition with KO*t*Bu resulting in **XXII**. The bis-vinyl amino ester **XXIII** was obtained by thermolytic elimination of the two phenyl sulfoxide groups. From there, amino ester **XXV** was accessed *via* saponification followed by esterification with 3-fluoropropanol. Picolinic acid **XXVII** was obtained by decomposition of carboxylic acid **XVIII** over 2 steps *via* Curtius rearrangement and hydrolysis. Remarkably, attempts for a direct hydrolysis of amide **XVIII** failed. [³H]RoSMA-18-precursor was then successfully synthesized *via* amide bond formation of picolinic acid **XXVII** and bis-vinyl amino ester **XXV**.



Scheme 4: Synthesis of [³H]RoSMA-18-precursor *via* bis-vinyl amino ester **XXIII** and picolinic acid **XXVII**.

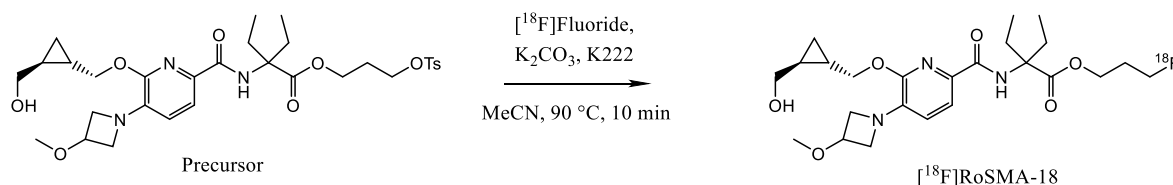
The tritiated probe [³H]RoSMA-18 was obtained by tritium enriched hydrogenation of the bis-olefin precursor in DMF (**Scheme 5**). An amount of 4.59 GBq of the [³H]RoSMA-18 was obtained with a radiochemical purity of 98.5% and a molar activity of 4.17 GBq/ μ mol, as determined by MS spectrometry.



Scheme 5: Radiosynthesis of [³H]RoSMA-18.

Fluorine-18 Radiochemistry

The tosylate precursor was synthesized *via* esterification of **XVIII** as outlined in **Scheme 3**. The radiofluorinated probe, codenamed [¹⁸F]RoSMA-18, was obtained by nucleophilic substitution using [¹⁸F]KF/Kryptofix₂₂₂ in acetonitrile (**Scheme 6**). Molar activities ranged from 52 - 65 GBq/ μ mol and the radiochemical purity was > 99%. The decay-corrected radiochemical yield was $10.6 \pm 3.8\%$ ($n = 16$). The crude product was purified by semipreparative HPLC, trapped on a C-18 Sep-Pak cartridge, and eluted with ethanol. The final formulation for biological evaluations was prepared with 5% ethanol in water for injection (WFI). The identity of the final product was confirmed by HPLC co-injection of the respective non-radioactive reference compounds.



Scheme 6: Radiosynthesis of [¹⁸F]RoSMA-18.

LogD_{7.4} determination

A mean LogD_{7.4} value of 1.7 ± 0.4 ($n = 4$) was determined for [¹⁸F]RoSMA-18 using the shake-flask method³³. The partition coefficient for non-radioactive reference **11** was assessed according to the recently reported carrier mediated distribution system (CAMDIS) method and amounted to 3.85^{33,34}.

In vitro autoradiography

CB2 specificity of [¹⁸F]RoSMA-18 was assessed by *in vitro* autoradiography using CB2-positive rat spleen tissues. In accordance with reported CB2 expression patterns in splenic lymphocytes, a high spleen binding was observed under baseline conditions, which was significantly reduced by $71 \pm 2\%$ ($n = 4$) following the addition of commercially available CB2 ligand GW-405,833 (10 μM), thus confirming the specificity of [¹⁸F]RoSMA-18 towards CB2 (**Figure 3A**). The CB2 specificity was further confirmed on rat and mouse spleen tissue with the tritium-labeled analogue, [³H]RoSMA-18 (**Figure 3B**). Considering the relatively high CB2 B_{max} of 697 ± 30 fmol/mg in the rodent spleen, a B_{max}/K_i ratio of 996 can be calculated for [¹⁸F]RoSMA-18, while a ratio >10 is considered appropriate for specific receptor imaging³⁵. Notably, when [³H]RoSMA-18 was employed on spleen tissue originating from CB2 knockout (ko) mice, tissue binding virtually disappeared. These results underline the high specificity of [³H]RoSMA-18 for CB2 receptors. In contrast to the spleen autoradiograms, CB2-negative brain slices of healthy Wistar rats did not reveal any specific tissue binding of [¹⁸F]RoSMA-18 (**Figure 4**). The latter findings were expected given that CB2 is hardly detectable in the healthy brain ($B_{\text{max}}/K_i \ll 10$).

To further elucidate the clinical relevance, post-mortem sections of human spinal cord tissue were evaluated for their CB2 protein expression levels by *in vitro* autoradiography using post-mortem human spinal cord tissues (**Figure 5**).

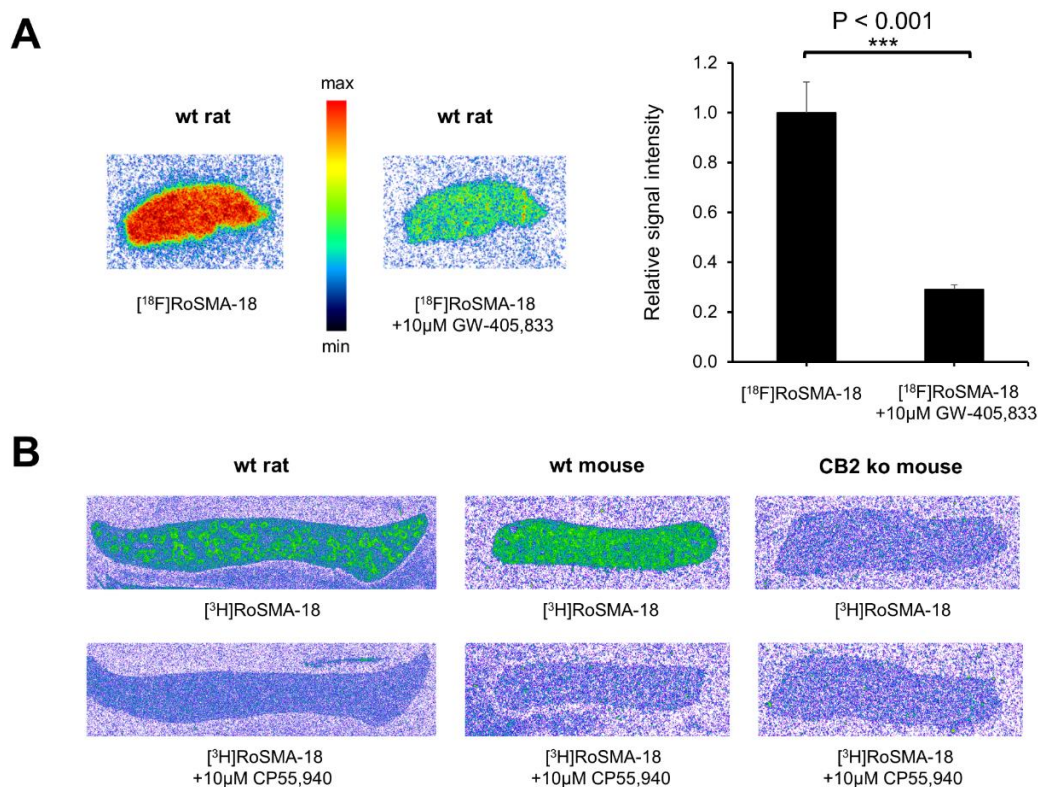


Figure 3: Representative *in vitro* autoradiography of the rodent spleen. **A.** Autoradiograms after incubation with either [^{18}F]RoSMA-18 only or in combination with excess CB2 ligand GW-405,833 (10 μM). Quantification revealed a specificity of $71 \pm 2\%$ ($n = 4$). **B.** Autoradiograms after incubation with [^3H]RoSMA-18 alone or in combination with excess CB2 ligand CP55,940 (10 μM) confirmed the high CB2 specificity in rat (80% signal reduction) and mouse (92% signal reduction). The specificity of the signal was confirmed by a 92% reduced binding to CB2 knockout mouse spleen tissue. wt, wild type. ko, knockout.

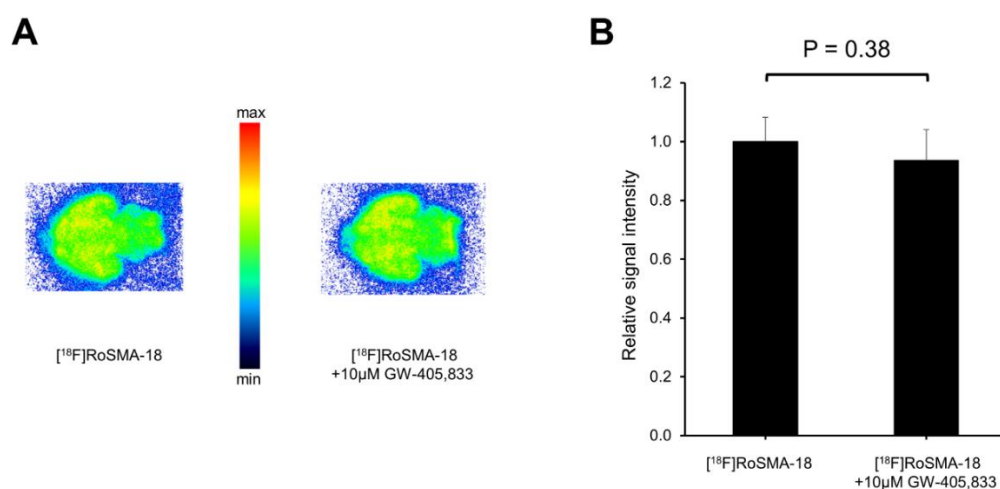


Figure 4: Representative *in vitro* autoradiography of the Wistar rat brain. **A.** Autoradiograms after incubation with either [^{18}F]RoSMA-18 only or in combination with excess CB2 ligand GW-405,833 (10 μM). **B.** Autoradiographic data quantification revealed no evident specific tissue binding in the healthy rat brain ($n = 4$).

An increased binding of [^{18}F]RoSMA-18 was observed in the diseased tissue, providing evidence for CB2 upregulation in neurodegenerative ALS patient's spinal cord. Addition of GW-405,833 (10 μM) led to a reduction of tracer binding confirming CB2 specificity. These findings are in accordance with previous reports on activated CB2-overexpressing microglial cells in patients suffering from ALS ³⁶.

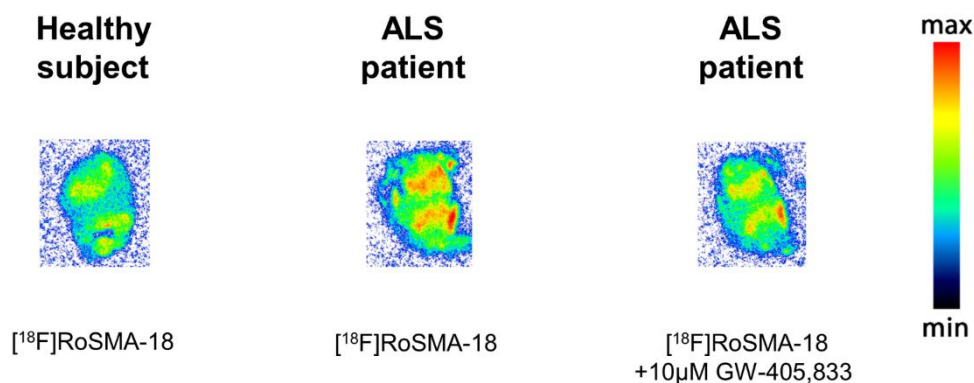


Figure 5: Representative *in vitro* autoradiograms of [^{18}F]RoSMA-18 on post-mortem human spinal cord sections (amyotrophic lateral sclerosis - ALS - patient vs. healthy control). For blockade conditions, CB2 ligand GW-405,833 was used in a concentration of 10 μM . Higher [^{18}F]RoSMA-18 binding was found in the diseased tissue compared to the healthy control, which was reduced under blockade conditions.

***Ex vivo* biodistribution**

Encouraged by the remarkable CB2-specificity observed in the autoradiograms, [^{18}F]RoSMA-18 was administered to Wistar rats and organ biodistribution was determined 30 min post injection. Highest tracer accumulation was detected in the intestine, urine and spleen. Intestinal and urinary uptake was not reduced under blockade (GW-405,833, 2 mg/kg) conditions, suggesting that the clearance of [^{18}F]RoSMA-18 and its radiometabolites is mainly *via* the hepatobiliary and renal pathways. In contrast, radioactivity in the spleen was reduced by an average of $86 \pm 2\%$ ($n = 4$) under blockade conditions, demonstrating specific target engagement *in vivo* (**Figure 6**). In accordance with autoradiographic findings, there was no specific binding in the healthy Wistar rat brain *in vivo*. Specific binding was further observed in the blood ($60 \pm 9\%$), the lung ($50 \pm 9\%$) and the femur ($49 \pm 18\%$). The latter findings are in line with previous reports on CB2 expression in circulating leukocytes ³⁷, bone marrow derived B-lymphocytes ³⁸ and lung-resident macrophages ³⁹

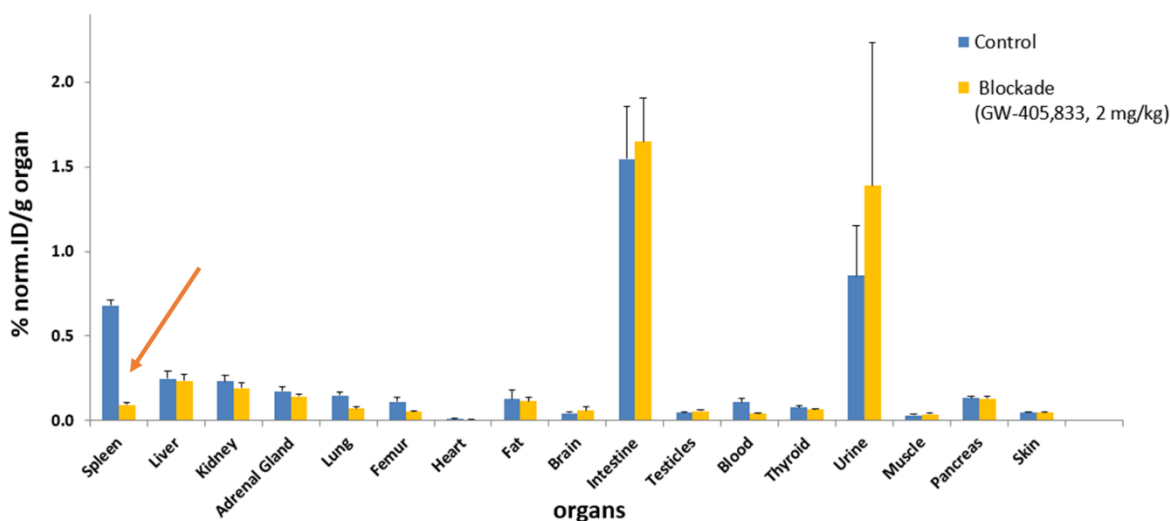


Figure 6: *Ex vivo* biodistribution of [^{18}F]RoSMA-18 in Wistar rats ($n = 4$). Animals were euthanized at 30 min post injection. A specificity of $86 \pm 2\%$ ($n = 4$) was observed for the spleen (highlighted by red arrow). Results are presented as % normalized injected dose per gram organ tissue. No specific binding was found in the brain. High unspecific uptake in urine and intestine suggest a combination of renal as well as hepatobiliary elimination of radioactivity.

PET and *in vivo* displacement

Upon tail-vein injection of 12 - 17 MBq (0.14 - 0.48 nmol) [^{18}F]RoSMA-18 into Wistar rats, time-activity curves were determined for the spleen - presented as standardized uptake values (SUV) from 0-60 min post injection (**Figure 7**). Radioactivity in the spleen reached a maximum SUV of 3.4 ± 0.3 ($n = 3$) at 15 min post injection and remained constant for additional 30 min, followed by a slow washout. To assess whether CB2 binding in the spleen is reversible, the CB2-specific partial agonist GW-405,833 (1.5 mg/kg) was administered as a bolus 10 min after tracer administration. Significant tracer displacement was observed consistently for all three animals treated with GW-405,833. At the last time point measured, baseline animals revealed an averaged SUV of 2.9 ± 0.6 while the displacement group exhibited a significantly reduced averaged SUV of 1.1 ± 0.5 ($P = 0.016$). These results show that [^{18}F]RoSMA-18 binds specifically and reversibly to CB2 receptors *in vivo*.

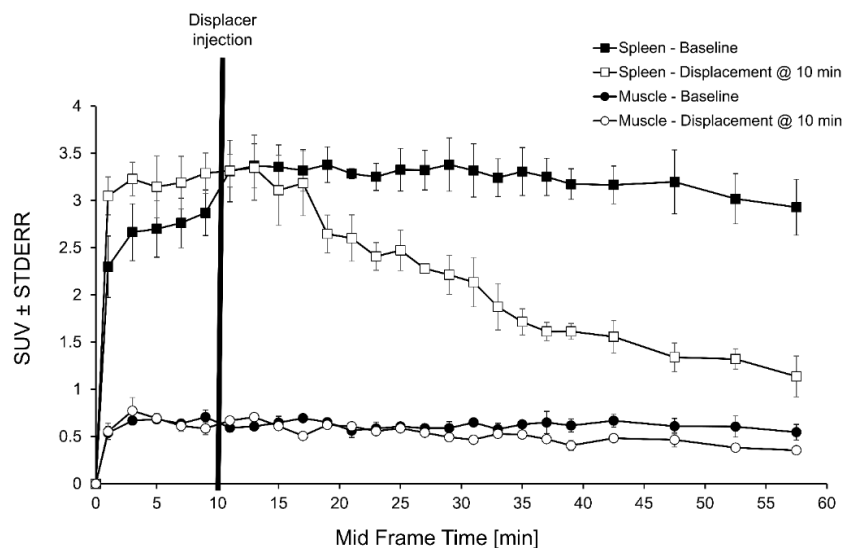


Figure 7: Time-activity curves of $[^{18}\text{F}]\text{RoSMA-18}$ are presented as standardized uptake values (SUV) \pm standard error (STDERR) for the rat spleen under baseline and displacement conditions. GW-405,833 (1.5 mg/kg) was administered 10 min after tracer injection (both intravenous). Significant displacement was observed for all tested animals (baseline $n = 3$, displacement $n = 3$).

Metabolite studies

Ex vivo metabolite studies were performed with four male Wistar rats by intravenous injection of the radiotracer (394 - 426 MBq) to determine intact tracer fraction in the plasma over time, and to assess the presence or absence of radiometabolites in the brain. Plasma samples were harvested at the time points of 5, 15, 30 and 45 min post injection. Fractions of intact parent radioligand in the plasma are depicted in **Table 2**. Two polar radiometabolites were identified in the plasma, however, only intact tracer was present in the brain samples, which were harvested at 5 and 45 min post injection. These findings suggest that radiometabolites are formed outside the CNS and do not enter the brain.

Table 2: Percentage of intact $[^{18}\text{F}]\text{RoSMA-18}$ in plasma and brain samples of Wistar rats at 0, 5, 15, 30 and 45 min p.i.

Time (min)	Plasma		Brain	
	$[^{18}\text{F}]\text{RoSMA-18}$ (%)	Radio-metabolites (%)	$[^{18}\text{F}]\text{RoSMA-18}$ (%)	Radio-metabolites (%)
0	100	0	not determined	
5	69	31	100	-
15	46	54	not determined	
30	31	69	not determined	
45	26	74	100	-

1
2
3 Although RoSMA-18 was chemically stable in solutions of varying pH and at elevated temperatures,
4 the fluoropropyl in [^{18}F]RoSMA-18 can potentially be cleaved by the action of enzymes, thereby
5 releasing 3- ^{18}F fluoropropanol or oxidized derivatives. These small radioactive fragments are
6 susceptible to defluorination, which can lead to an accumulation of radioactive fluoride in the bone
7 mineral matrix. In particular, the latter is critical for neuroimaging due to the close proximity of the skull
8 to adjacent brain regions such as the cortex or cerebellum. Radioactivity spill-over from the skull to
9 adjacent brain regions complicates data analysis. To assess potential defluorination, we investigated the
10 metabolic stability using microsomes and identified the carboxylic acid metabolite depicted in **Figure**
11 **8** by LC-MS/MS. Notably, despite steric hinderance, the fluorine-bearing side chain was efficiently
12 cleaved by rat and human liver enzymes *in vitro* (**Figure 8**), suggesting that compound RoSMA-18 and
13 its radioactive analogue, [^{18}F]RoSMA-18, may indeed be susceptible to *in vivo* defluorination.

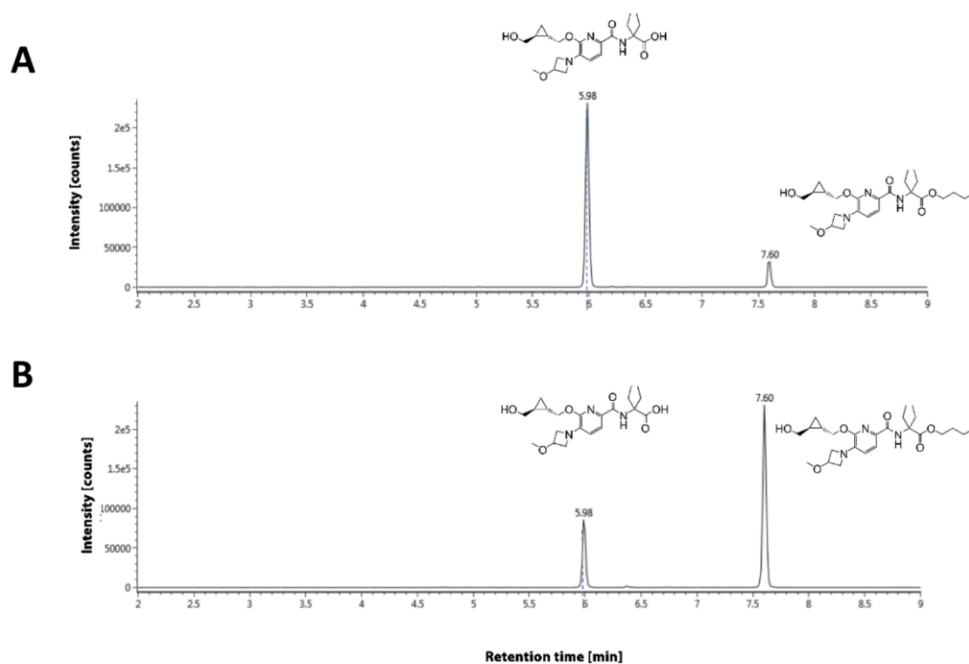
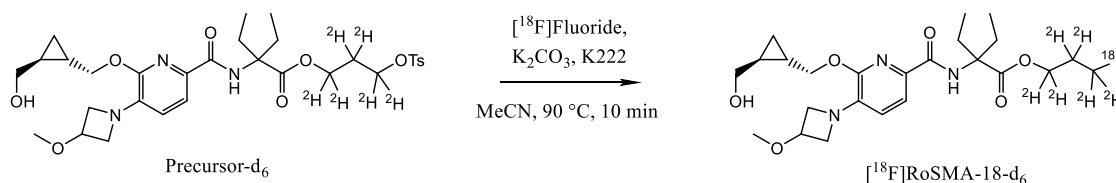


Figure 8: Extracted mass chromatograms of RoSMA-18 and its dealkylated metabolite formed after 30 min of incubation with (A) rat and (B) human liver microsomes.

14
15
16 In accordance with the metabolite identification results described above, we found substantial
17 radioactivity accumulation *in ventral* as well as dorsal skull segments during PET studies of
18 [^{18}F]RoSMA-18 in Wistar rats (**Figure 9A**). It has been previously reported that terminal fluoropropoxy
19 moieties can be subjected to enzyme-mediated defluorination^{40, 41}. Initial studies indicated an oxidative

mechanism leading to a dealkylation of the ester. To overcome this limitation, we replaced all the hydrogen atoms of the fluoropropyl side chain with deuterium atoms. The radiosynthesis of [^{18}F]RoSMA-18-d₆ was performed under identical conditions as with non-deuterated [^{18}F]RoSMA-18 (Scheme 7). Indeed, the deuteration strategy led to a remarkable reduction of radioactivity uptake *in ventral* and dorsal skull regions, confirming the hypothesis that a deuterated fluoropropyl side chain reduces enzyme-mediated defluorination compared to its hydrogen-bearing analogue (Figure 9B).



Scheme 7: Radiosynthesis of [^{18}F]RoSMA-18-d₆.

Due to the low abundance of CB2 receptors in the healthy rat brain, however, the time-activity curve revealed a fast washout of [^{18}F]RoSMA-18-d₆ (Supplemental Figure 5).

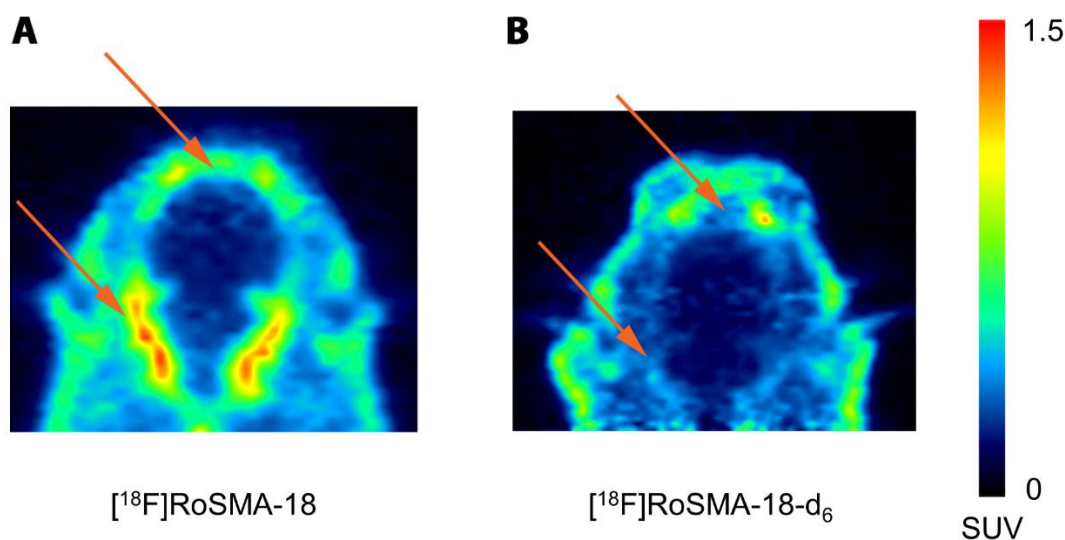


Figure 9: Coronal PET images of the head region averaged from 0-60 min post injection are presented after tail-vein injection of either [^{18}F]RoSMA-18 (panel A) or [^{18}F]RoSMA-18-d₆ (panel B) into Wistar rats. Results are presented as standardized uptake values (SUV). Lateral and dorsal skull regions are highlighted by arrows. Skull radioactivity is significantly reduced in the animal scanned with [^{18}F]RoSMA-18-d₆, indicating diminished defluorination of the deuterated tracer *in vivo*.

In vitro metabolite identification studies of RoSMA-18-d₆ revealed a remarkably reduced dealkylation by rat (Figure 10A) and human liver microsomes (Figure 10B), as compared to RoSMA-18.

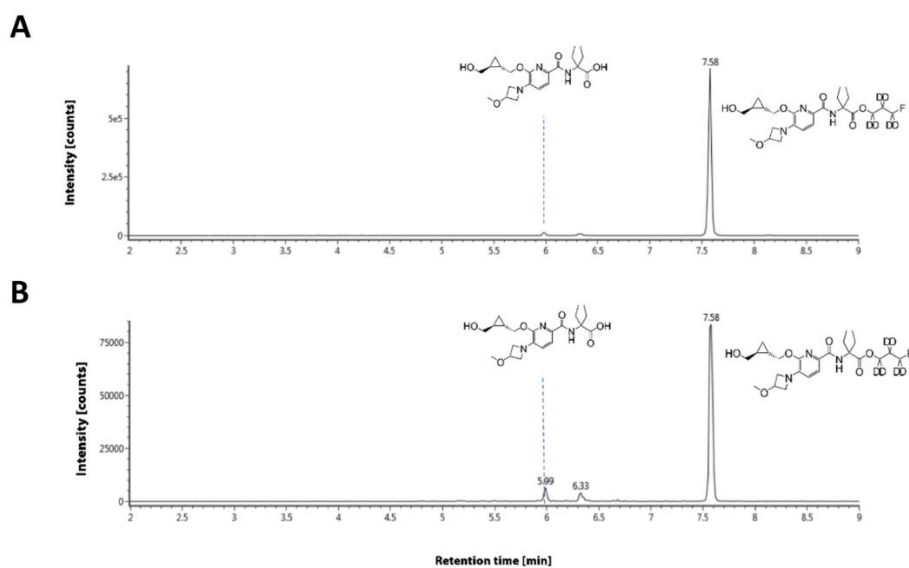


Figure 10: Extracted mass chromatograms of RoSMA-18-d₆ and its dealkylated metabolite formed after 30 min of incubation with (A) rat and (B) human liver microsomes.

Although isotopic exchange should not affect pharmacodynamic properties, we determined the binding affinity of RoSMA-18-d₆ for CB2 and its selectivity over CB1. Applying identical experimental conditions as with RoSMA-18, an inhibitory constant (K_i) of 0.8 ± 0.4 nM ($n = 4$) towards human CB2 was found for the deuterated form, RoSMA-18-d₆, which is identical to the K_i value of 0.7 nM for the non-deuterated form. In addition, a K_i value of > 10 μ M towards human CB1 was obtained for RoSMA-18-d₆, thus confirming the high selectivity over CB1. For other species such as mouse, rat and cynomolgus monkey, the K_i values obtained for RoSMA-18-d₆ were 1.2 ± 0.3 nM, 0.3 ± 0.3 nM and 0.6 ± 0.3 nM, respectively. Moreover, we extended the autoradiographic findings by showing that [¹⁸F]RoSMA-18 and its deuterated analogue, [¹⁸F]RoSMA-18-d₆, provide essentially identical *in vitro* autoradiograms. This was the case for the rat spleen and the rat brain, with substantial CB2 specificity detected in the spleen but not in the brain (**Figures 11 and 12**, respectively).

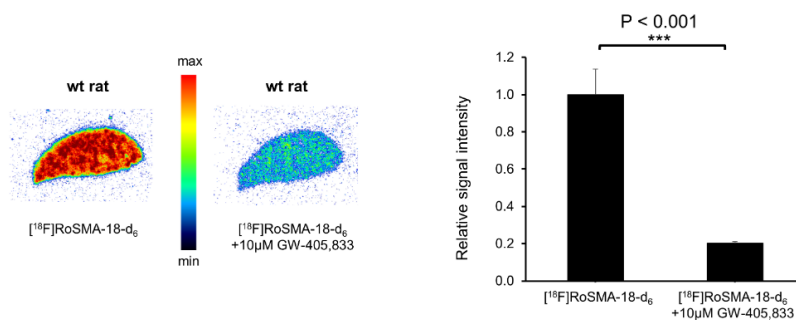


Figure 11: Representative *in vitro* autoradiography of [^{18}F]RoSMA-18- d_6 using rodent spleen. Autoradiograms after incubation with either [^{18}F]RoSMA-18- d_6 only or in combination with GW-405,833 (10 μM). Quantification of the data confirmed the high CB2 specificity ($n = 4$).

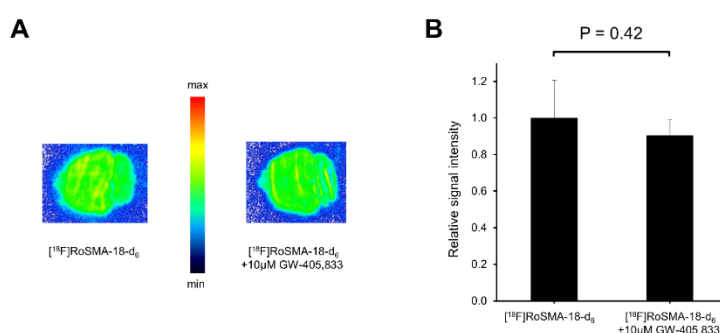


Figure 12: Representative *in vitro* autoradiography of [^{18}F]RoSMA-18- d_6 using rodent brain. **A.** Autoradiograms after incubation with either [^{18}F]RoSMA-18- d_6 only or in combination with GW-405,833 (10 μM). **B.** Quantification of the data confirmed the lack of CB2-specific binding in the healthy rat brain ($n = 4$).

To further show that [^{18}F]Ro-SMA-18- d_6 can detect CB2 upregulation in the human spinal cord, we conducted *in vitro* autoradiography experiments, thereby performing data quantification and statistical analysis ($n = 4$). It was found that CB2 expression was significantly higher in post-mortem ALS spinal cord tissues compared to the control tissues (**Figure 13**, quantification in the grey matter). This signal was significantly reduced by blockade with either GW-405,833 or the previously reported selective CB2 ligand RSR-056 with the same structural scaffold (K_i hCB2: 2.5 nM)⁴². There was no significant difference between the blockade by GW-405,833 and RSR-056, supporting the lack of off-target binding by [^{18}F]RoSMA-18- d_6 .

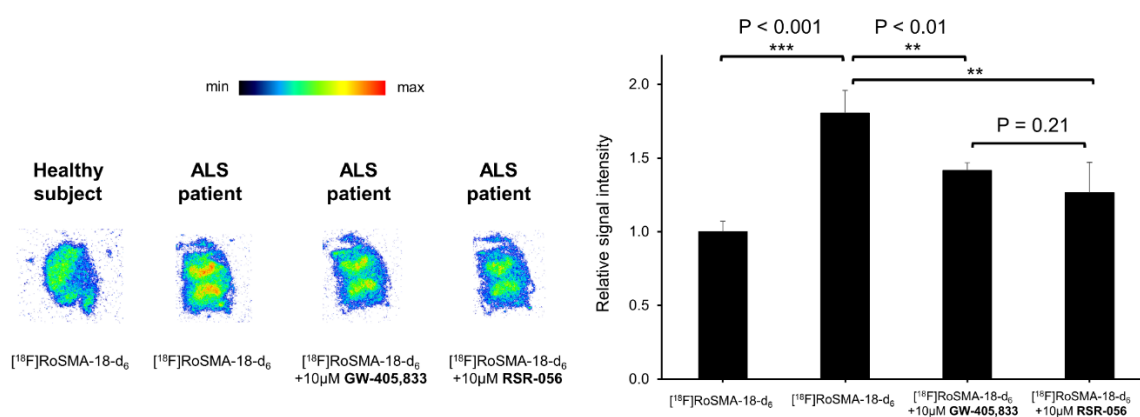


Figure 13: Representative *in vitro* autoradiography of [¹⁸F]RoSMA-18-d₆ using post-mortem human ALS and control spinal cord tissue. Autoradiograms are presented after incubation with either [¹⁸F]RoSMA-18-d₆ only or in combination with GW-405,833 (10 μM) or RSR-056 (10 μM), respectively. Quantification of the data confirmed CB2 upregulation in the grey matter of ALS patient tissues compared to healthy control sections (n = 4).

Discussion

Structure-activity relationship studies led to the discovery of RoSMA-18, a highly potent (K_i for hCB2 = 0.7 nM) fluorinated CB2 ligand that displayed an outstanding selectivity factor of > 12'000 over CB1, thereby substantially outperforming the previously reported lead compound [¹⁸F]**3** (selectivity factor <700 over CB1)²⁹. The high selectivity over CB1 is particularly relevant with respect to CB2-targeted brain imaging, since CB1 is known to be highly expressed in the CNS⁴³. Due to the promising properties, RoSMA-18 was selected for radiofluorination and the respective tosylate precursor was synthesized. Of note, our initial concerns about the diminishing role of a non-protected hydroxyl-group of the tosylate precursor on radiosynthesis outcome proved to be unfounded. A robust radiosynthetic procedure was established that yielded the designated radioligand in excellent pharmaceutical quality for biological evaluation. Significant differences in the lipophilicity values of RoSMA-18 and the respective radiofluorinated analogue, [¹⁸F]RoSMA-18, were observed. We attribute this discrepancy to the different experimental methods used for the determination of the logD_{7.4} values. Whereas the logD_{7.4} value of RoSMA-18 was determined by the recently reported carrier mediated distribution system (CAMDIS)^{33,34}, the value for [¹⁸F]RoSMA-18 was obtained by the widely used shake-flask method⁴⁴. An identical average logD_{7.4} value of 1.7 was obtained by the shake-flask method for [¹⁸F]RoSMA-18

1
2
3 and its deuterated analogue, [^{18}F]RoSMA-18- d_6 . This value compares well to previously reported brain
4 penetrating probes and lies within the recommended range of 1 – 3 suggested by Waring et al. ⁴⁵.
5
6

7
8 [^{18}F]RoSMA-18 exhibited outstanding specificity for CB2-positive spleen by *in vitro* autoradiography,
9 *in vivo* PET and *ex vivo* biodistribution. Compared to the previously reported lead compound [^{18}F]**3**,
10 [^{18}F]RoSMA-18 displayed a substantial increase in specific spleen binding by *in vitro* autoradiography
11 ([^{18}F]**3** vs. [^{18}F]RoSMA-18, 31% vs. 71%) as well as by *in vivo* PET displacement studies ²⁹. Indeed,
12 spleen uptake was approximately 3-fold higher for [^{18}F]RoSMA-18 than [^{18}F]**3** from 15-60 min after
13 radioligand injection into Wistar rats primarily because [^{18}F]**3** exhibited a rapid washout from the spleen,
14 while [^{18}F]RoSMA-18 spleen binding remained at a high level during the whole scanning period of 60
15 min ²⁹. In accordance with previous reports, we did not detect any CB2 in the healthy rodent brain,
16 neither *in vitro* nor *in vivo* ⁴⁶. With regard to the clinical relevance of CB2-imaging, we were able to
17 show that [^{18}F]RoSMA-18 can be used to image CB2 receptor upregulation in ALS using
18 autoradiography on post-mortem human spinal cord sample tissues. ALS is a fatal neurodegenerative
19 disorder affecting motor neurons and with no current effective treatment ⁴⁷. Its etiology is not yet
20 understood, and early disease detection is hampered by a challenging differential diagnosis often leading
21 to false positive results. PET experiments with [^{18}F]RoSMA-18 has the potential to become a valuable
22 tool for non-invasive patient diagnosis and further help to understand ALS disease etiology.
23
24
25
26
27
28
29
30
31
32
33
34
35
36
37
38
39
40

41 To study the *in vivo* stability of [^{18}F]RoSMA-18, we analyzed plasma and brain samples at predefined
42 time points after radioligand injection into Wistar rats. Two polar radiometabolites were detected in the
43 plasma samples and only intact [^{18}F]RoSMA-18 was found in the brain samples. We therefore conclude
44 that the radiometabolites are formed outside the CNS and do not cross the blood-brain barrier. This is
45 particularly relevant as radiometabolites complicate image analysis and thus are not desired in CNS-
46 based PET. Despite initial promising chemical stability results, a relatively high skull radioactivity
47 uptake was observed, possibly owing to *in vivo* enzymatic defluorination and subsequent accumulation
48 of radioactive fluoride in the bone mineral matrix. Consequently, a considerable spill-over effect was
49 observed, which was most pronounced in the cerebellar region. A strategy of deuteration was proposed
50 to overcome the limitation, and hence, all the hydrogen atoms in the fluoropropyl side chain were
51
52
53
54
55
56
57
58
59
60

1
2
3 replaced with deuterium atoms. This strategy abolished radioactivity uptake in lateral and dorsal skull
4 regions as confirmed by the respective PET images and supports the hypothesis that a deuterated
5 fluoropropyl side chain prevents enzyme-mediated defluorination. Metabolite identification studies
6 confirmed the improved stability of RoSMA-18-d₆ towards enzymatic degradation. Further, the
7 subnanomolar affinity for CB2 and the outstanding selectivity over CB1 were confirmed for the
8 deuterated version, paving the way for the assessment of inflammatory CB2 upregulation in the
9 mammalian CNS.
10
11
12
13
14
15
16
17
18

19 Conclusion

20
21
22 In the present study, we performed a structure-activity relationship of fluorinated pyridine-based CB2
23 ligands starting from the previously reported lead compound [¹⁸F]**3**. RoSMA-18 emerged as the most
24 promising candidate, exhibiting a subnanomolar affinity (K_i for hCB2 = 0.7 nM) and a remarkable
25 selectivity factor of > 12'000 over CB1, which substantially outperformed [¹⁸F]**3** (K_i for hCB2 = 6 nM
26 and selectivity factor of 698)²⁹. [¹⁸F]RoSMA-18 proved to be highly specific/selective in autoradiograms
27 of CB2-positive rat spleen. We further showed that [¹⁸F]RoSMA-18 can be used to image CB2 receptor
28 upregulation in ALS patients by autoradiography on post-mortem human spinal cord samples. *In vivo*
29 evaluation of the [¹⁸F]RoSMA-18 in the CB2-positive spleen revealed a specificity of 86 ± 2%. *In vivo*
30 defluorination of [¹⁸F]RoSMA-18 was circumvented by the replacement of all the hydrogen atoms in
31 the fluoropropyl side chain with deuterium atoms to afford [¹⁸F]RoSMA-18-d₆. Overall, these results
32 suggest that [¹⁸F]RoSMA-18-d₆ is a promising CB2 PET radioligand for clinical translation.
33
34
35
36
37
38
39
40
41
42
43
44
45
46
47
48

49 Experimental section

50
51 Wistar rats were purchased from Charles River (Sulzfeld, Germany) and kept under standard conditions.
52 All animal studies were carried out in accordance with the Swiss Animal Protection Law as well as the
53 ARRIVE guidelines and further approved by the local veterinary office in Zurich, Switzerland. Post-
54 mortem human spinal cord tissue of healthy controls and ALS patients were kindly provided by the
55 Cantonal Hospital St. Gallen (Switzerland) with a written consent of the donors.
56
57
58
59
60

1
2
3 Reagents and solvents were purchased from Sigma Aldrich Chemie GmbH (Germany), Acros Organics
4 (Belgium), ABCR GmbH (Germany), Merck (Germany) or Fluka (Switzerland) and were used without
5 further purification. A Bruker Avance FT-NMR spectrometer (300 or 600 MHz) was used to record ¹H-
6 and ¹³C-NMR spectra and the chemical shifts (δ) are given in ppm referenced to tetramethylsilane (TMS,
7 0 ppm). Coupling constants (J) are presented in Hz and multiplicities in the ¹H NMR spectra are reported
8 as either s = singlet, d = doublet, t = triplet, m = multiplet or br = broad peak. Mass spectrometry (MS)
9 was carried out on a Bruker's maXis (ESI-Qq-ToF-MS) spectrometer (Bruker Daltonik GmbH,
10 Germany) and MS results are reported in m/z. Purity of target compound was assessed by HPLC and
11 was at least > 95%. [¹⁸F]RoSMA-18 and [¹⁸F]RoSMA-18-d₆ were purified by semi-preparative HPLC
12 (Merck-Hitachi L2130 system), equipped with a radiation detector VRM 202 (Comecer, Netherlands)
13 in combination with an ACE 5 C-18-300 (250 x 10.0 mm, 5 μ m) column and a gradient solvent system.
14 The following system was used for semipreparative purifications: 0.1% H₃PO₄ in H₂O (solvent A),
15 MeCN (solvent B); 0.0-8.0 min, 20% B; 8.1-30.0 min, 20-90% B; 30.1-35.0 min, 90% B; 35.1-37.0 min,
16 90-20% B; 37.1-43.0 min, 20% B. A flow rate of was 4 mL/min was used. The UV signal detection was
17 conducted at 230 nm. Analytical quality control was performed on an Agilent 1100 series HPLC system,
18 equipped with UV detector and a GabiStar radiodetector (Raytest). A reverse phase ACE C18-AR
19 column (50 x 4.6 mm, 3 μ m) was used for analytical quality control, in combination with the following
20 separation conditions: 0.1% TFA in H₂O (solvent A), MeCN (solvent B); 0.0-2.0 min, 20% B; 2.1-12.0
21 min, 20-90% B; 12.1-14.0 min, 90% B; 14.1-15.0 min, 90-20% B; 15.1-20.0 min, 20% B. The flow rate
22 was 1 mL/min and the UV signal was recorded at 320 nm. Molar activities were calculated by comparing
23 the UV intensity of the formulated products with calibration curves of the respective standards.
24
25
26
27
28
29
30
31
32
33
34
35
36
37
38
39
40
41
42
43
44
45
46
47

48 **Chemistry**

49
50
51 General procedure for the ether formation reactions yielding compounds **1**, **2**, **5**, **7**, **8**, **15**:

52 To a solution of the respective alcohol in DMF (62-133 mM) was added NaH (2-5 equiv.) at 0 °C. The
53 resulting reaction mixture was stirred at ambient temperature for 30 min before the corresponding halide
54 (5 equiv.) was added. The reaction mixture was stirred at RT for 0.5-28 h. The solvent was evaporated
55 under reduced pressure and the residue diluted with EtOAc. The organic phase was extracted with brine,
56
57
58
59
60

1
2
3 dried over Na₂SO₄ and concentrated *in vacuo*. Column chromatography with variable eluent systems
4 consisting of heptane/EtOAc was performed to obtain the title compounds generally in low yields as
5 depicted in **Schemes 1-2**.
6
7
8
9

10
11 General procedure for fluorination reactions yielding compounds **3, 4** and **6**:

12
13 A solution of the respective mesylate precursor in acetonitrile (12-37 mM) was combined with tetra
14 butyl ammonium fluoride in tetrahydrofuran (5 equiv.) under argon atmosphere. The resulting mixture
15 was stirred at 80 °C for 1-16 h. The reaction mixture was diluted with ethyl acetate and extracted 3x
16 with aqueous HCl (1M) and 1x with brine. Column chromatography with variable eluent systems
17 consisting of heptane/EtOAc was carried out to obtain the title compounds variable yields (**Scheme 2**).
18
19
20
21
22
23
24
25

26 General procedure for esterifications to give compounds **9, 10, 11, 12, 13, 14**:

27
28 A solution of the appropriate carboxylic acid in DMF (40 mM) was combined with K₂CO₃ (3 equiv.),
29 followed by the addition of the respective halide (3-5 equiv.). The resulting mixture was stirred at room
30 temperature for 2-4 h. Volatiles were removed *in vacuo* and the resulting crude was diluted with EtOAc.
31 The organic layer was extracted with brine, dried over Na₂SO₄ and concentrated *in vacuo*. Silica column
32 chromatography with eluent systems of variable heptane/EtOAc combinations gave the title compounds
33 in yields that are shown in **Scheme 3**.
34
35
36
37
38
39

40 General procedure for esterifications yielding the **precursor and precursor-d₆**:

41
42 To a solution of the respective carboxylic acid in DMF (12-24 mM) was added potassium carbonate (3
43 equiv.) and the appropriate ditosylate (2-3 equiv.). The reaction mixture was stirred for 16-17 h at
44 ambient temperature, subsequently diluted with water and extracted 3x with ethyl acetate. The combined
45 organic layers were extracted with brine, dried and evaporated under reduced pressure. Silica column
46 chromatography with eluent systems of variable hexane/EtOAc combinations gave the title compounds.
47
48
49
50
51
52
53
54

55 General procedure for Buchwald-Hartwig aminations to give compounds **I, X, XV**:

56
57 To a solution of the appropriate brominated precursor in toluene (31-72 mM) was added the
58 corresponding amine (1.5 equiv.), Cs₂CO₃ (3 equiv.), *rac*-BINAP (0.2 equiv.) and [Pd(OAc)₂] (0.2
59
60

1
2
3 equiv.) and the reaction mixture was stirred at 110 °C for 1-3 h. The reaction mixture was diluted with
4
5 EtOAc and filtered through Celite. Subsequently, the organic phase was washed 3x with aqueous HCl
6
7 (1 M) and 1x with brine, then dried over Na₂SO₄. Column chromatography was performed with gradient
8
9 elution using a system of heptane/EtOAc to give the title compounds in yields very good yields ranging
10
11 from 85-87% (**Scheme 2**).

12
13
14
15
16 General procedure for the formation of methoxy-pyridines **III**, **VII**, **XII**:

17
18 To a solution of the respective alcohol in DMF (53-141 mM) was added NaH (3 equiv.) at 0 °C. The
19
20 resulting reaction mixture was allowed to stir at ambient temperature for 30 min before 1.4-1.5 equiv.
21
22 of the respective alcohol was added and the reaction mixture was stirred at room temperature (or 80 °C)
23
24 for 3-16 h according to **Scheme 2**. The volatiles were removed under reduced pressure and the residue
25
26 diluted with EtOAc. The organic phase was extracted with brine, dried over Na₂SO₄ and concentrated
27
28 under reduced pressure. Column chromatography with variable eluent systems consisting of
29
30 heptane/EtOAc was performed to obtain the title compounds.

31
32
33
34
35 General procedure for the amide coupling reactions yielding compounds **IV**, **VIII**, **XIII**:

36
37 To the appropriate picolinic acid in DMF (16-228 mM) was added DIPEA (3-5 equiv.) and TBTU (1.0
38
39 – 1.2 equiv.), followed by the addition of ethyl 2-amino-2-ethylbutanoate (1.2-2.0 equiv.). Subsequently,
40
41 the reaction mixture was stirred at ambient temperature for 1-28 h, depending on starting material
42
43 consumption monitored by TLC. The volatiles were removed under reduced pressure and the resulting
44
45 crude was subsequently diluted with EtOAc. The organic layer was extracted with brine, dried over
46
47 Na₂SO₄ and concentrated under reduced pressure. Column chromatography using variable combinations
48
49 of heptane and EtOAc gave the title compounds as depicted in **Scheme 2**.

50
51
52
53
54 General procedure for saponification reactions yielding compounds **XVIII**, **XX**:

55
56 A solution of the appropriate ester in THF/MeOH/H₂O 1:1:1 (42-78 mM) was combined with KOH (5
57
58 equiv.) and the resulting mixture was stirred at 90 °C for 18 h. The organic solvents were removed under
59
60 reduced pressure. Subsequently, the aqueous phase was acidified (pH = 2) and extracted 3x with ethyl

1
2
3 acetate. The combined organic layers were extracted with brine and dried over Na₂SO₄. The organic
4
5 phase was evaporated *in vacuo* and the crude residue was purified by column chromatography using
6
7 varying combinations of hexane/ethyl acetate to give the title compounds with excellent yields as shown
8
9 in **Scheme 3**.

10
11
12
13 General procedure for mesylation reactions yielding compounds **V**, **IX**, **XIV**:

14
15 A solution of the respective alcohol precursor in DCM (97-111 mM) was combined with triethylamine
16
17 (3 equiv.) and mesyl chloride (2 equiv.) at 0 °C. The reaction mixture was stirred at ambient temperature
18
19 for 0.5-2 h and subsequently diluted with ethyl acetate. The organic layers were washed 3x with
20
21 saturated sodium hydrogen carbonate and 1x with brine. The combined organic layers were dried over
22
23 Na₂SO₄ and evaporated *in vacuo*. The crude residue was purified by column chromatography using
24
25 combinations of hexane/ethyl acetate to give the title compounds in quantitative yields as shown in
26
27
28 **Scheme 2**.

29
30
31
32 General procedures for alcohol deprotection reactions yielding **II**, **XI**, **XVI**:

33
34 **Compound II:** Silyl ether **I** was dissolved in a mixture of acetic acid, water and tetrahydrofuran (3:1:1,
35
36 71 mM) and the mixture was stirred at ambient temperature for 1 h. The organic solvents were removed
37
38 under reduced pressure and the crude residue was diluted with ethyl acetate. The organic layers were
39
40 extracted 3x with saturated aqueous NaHCO₃ and 1x with brine, dried over Na₂SO₄ and concentrated *in*
41
42 *vacuo*. The product was used without further purification for the subsequent step (purity by analytical
43
44 HPLC: 100%).

45
46
47
48
49 **Compounds XI and XVI:** To a solution of the respective ether in ethyl acetate/methanol (10:1, 37-61
50
51 mM) was added palladium on carbon (Pd-C, 4-5 equiv.) and the suspension was stirred under H₂
52
53 atmosphere for 48 h. The reaction mixture was filtered through Celite and the solvents were removed
54
55 under reduced pressure. The product was used without further purification for the subsequent step
56
57 (purity by analytical HPLC: 95-100%).
58
59
60

Ethyl 2-ethyl-2-(6-(((*cis*)-2-((fluoromethoxy)methyl)cyclopropyl)methoxy)-5-(3-methoxyazetidino-1-yl)picolinamido)butanoate (1)

¹H NMR (600 MHz, Chloroform-*d*) δ 8.63 (s, 1H), 7.64 (d, *J* = 7.9 Hz, 1H), 6.60 (d, *J* = 7.9 Hz, 1H), 5.32 (ddd, *J* = 56.8, 9.0, 1.9 Hz, 2H), 4.68 – 4.52 (m, 1H), 4.37 – 4.20 (m, 6H), 4.01 – 3.71 (m, 4H), 3.34 (s, 3H), 2.70 – 2.58 – 2.50 (m, 2H), 1.94 – 1.80 (m, 2H), 1.38 – 1.25 (m, 5H), 1.01 – 0.93 (m, 1H), 0.82 – 0.72 (m, 6H), 0.55 – 0.42 (m, 1H). LC-MS (ESI): 482.2657 [M+H⁺]; calculated for C₂₄H₃₆FN₃O₆ +H⁺: 482.2666.

Ethyl 2-ethyl-2-(6-(((*cis*)-2-((2-fluoroethoxy)methyl)cyclopropyl)methoxy)-5-(3-methoxyazetidino-1-yl)picolinamido)butanoate (2)

¹H NMR (600 MHz, Chloroform-*d*) δ 8.63 (s, 1H), 7.64 (d, *J* = 7.9 Hz, 1H), 6.60 (d, *J* = 7.9 Hz, 1H), 4.55 (dt, *J* = 47.7, 4.1 Hz, 2H), 4.40 – 4.19 (m, 7H), 3.68 (dt, *J* = 29.6, 4.2 Hz, 2H), 3.59 – 3.50 (m, 4H), 3.34 (s, 3H), 2.70 – 2.54 (m, 2H), 1.94 – 1.80 (m, 2H), 1.53 – 1.39 (m, 1H), 1.38 – 1.25 (m, 4H), 0.98 – 0.90 (m, 1H), 0.76 (t, *J* = 7.3 Hz, 6H), 0.50 – 0.41 (m, 1H). LC-MS (ESI): 496.3 [M+H⁺].

Ethyl 2-ethyl-2-(6-(((*cis*)-2-(fluoromethyl)cyclopropyl)methoxy)-5-(3-methoxyazetidino-1-yl)picolinamido)butanoate (3)

¹H NMR (600 MHz, Chloroform-*d*) δ 8.62 (s, 1H), 7.64 (d, *J* = 7.9 Hz, 1H), 6.60 (d, *J* = 7.9 Hz, 1H), 4.75 – 4.45 (m, 3H), 4.32 – 4.21 (m, 6H), 3.92 – 3.82 (m, 2H), 3.34 (s, 3H), 2.64 – 2.57 (m, 2H), 1.91 – 1.84 (m, 2H), 1.63 – 1.59 (m, 1H), 1.49 – 1.43 (m, 1H), 1.32 (t, *J* = 7.3 Hz, 3H), 1.02 – 0.95 (m, 1H), 0.79 – 0.74 (m, 6H), 0.57 – 0.52 (m, 1H). LC-MS (ESI): 452.2567 [M+H⁺]; calculated for C₂₃H₃₄FN₃O₅ +H⁺: 452.2561.

Ethyl 2-ethyl-2-(6-(3-fluoro-2,2-dimethylpropoxy)-5-(3-methoxyazetidino-1-yl)picolinamido)butanoate (4)

¹H NMR (600 MHz, Chloroform-*d*) δ 8.63 (s, 1H), 7.64 (d, *J* = 7.9 Hz, 1H), 6.60 (d, *J* = 7.9 Hz, 1H), 4.52 – 4.09 (m, 9H), 3.96 – 3.81 (m, 2H), 3.34 (s, 3H), 2.58 (dt, *J* = 14.7, 7.5 Hz, 1H), 1.88 (dq, *J* =

1
2
3 14.5, 7.3 Hz, 1H), 1.32 (t, $J = 7.3$ Hz, 3H), 1.16 – 1.06 (m, 6H), 0.76 (t, $J = 7.3$ Hz, 6H). LC-MS (ESI):
4
5 454.2719 [M+H⁺]; calculated for C₂₃H₃₆FN₃O₅ +H⁺: 454.2717.
6
7
8
9

10
11 **Ethyl 2-ethyl-2-(6-(3-(fluoromethoxy)-2,2-dimethylpropoxy)-5-(3-methoxyazetidino-1-**
12 **yl)picolinamido)butanoate (5)**
13
14

15
16 ¹H NMR (600 MHz, DMSO-*d*₆) δ 8.42 (s, 1H), 7.48 (d, $J = 7.9$ Hz, 1H), 6.73 (d, $J = 7.9$ Hz, 1H), 5.32
17
18 (d, $J = 56.8$ Hz, 2H), 4.31 – 4.14 (m, 7H), 3.87 – 3.76 (m, 2H), 3.65 – 3.45 (m, 2H), 3.24 (s, 3H), 2.35
19
20 (dt, $J = 14.7, 7.5$ Hz, 1H), 1.81 (dq, $J = 14.5, 7.3$ Hz, 1H), 1.23 (t, $J = 7.3$ Hz, 3H), 1.03 (s, 6H), 0.70
21
22 (t, $J = 7.3$ Hz, 6H). LC-MS (ESI): 483.2762 [M+H⁺]; calculated for C₂₄H₃₅FN₃O₆ +H⁺: 483.2745.
23
24
25

26 **Ethyl 2-ethyl-2-(6-(((*trans*)-2-(fluoromethyl)cyclopropyl)methoxy)-5-(3-methoxyazetidino-1-**
27 **yl)picolinamido)butanoate (6)**
28
29

30
31 ¹H NMR (600 MHz, DMSO-*d*₆) δ 8.39 (s, 1H), 7.47 (d, $J = 7.9$ Hz, 1H), 6.73 (d, $J = 7.9$ Hz, 1H), 4.44
32
33 – 4.11 (m, 9H), 3.87 – 3.73 (m, 2H), 3.24 (s, 3H), 2.39 – 2.35 (m, 2H), 1.87 – 1.75 (m, 2H), 1.37 – 1.30
34
35 (m, 2H), 1.23 (t, $J = 7.3$ Hz, 3H), 0.76 – 0.63 (m, 8H). LC-MS (ESI): 451.2496 [M+H⁺]; calculated for
36
37 C₂₃H₃₃FN₃O₅ +H⁺: 451.2482.
38
39

40 **Ethyl 2-ethyl-2-(6-(((*trans*)-2-((2-fluoroethoxy)methyl)cyclopropyl)methoxy)-5-(3-**
41 **methoxyazetidino-1-yl)picolinamido)butanoate (7)**
42
43

44
45 ¹H NMR (600 MHz, Chloroform-*d*) δ 8.63 (s, 1H), 7.64 (d, $J = 7.9$ Hz, 1H), 6.60 (d, $J = 7.9$ Hz, 1H),
46
47 4.55 (dt, $J = 47.7, 4.1$ Hz, 2H), 4.42 – 4.33 (m, 2H), 4.28 – 4.18 (m, 2H), 4.01 – 3.81 (m, 6H), 3.68 (dt,
48
49 $J = 29.6, 4.2$ Hz, 2H), 3.46 – 3.39 (m, 1H), 3.34 (s, 3H), 2.70 – 2.54 (m, 2H), 1.94 – 1.80 (m, 2H), 1.38
50
51 – 1.25 (m, 5H), 0.81 – 0.64 (m, 8H). LC-MS (ESI): 496.2825 [M+H⁺]; calculated for C₂₅H₃₈FN₃O₆ +H⁺:
52
53 496.2823.
54
55
56

57 **Ethyl 2-ethyl-2-(6-(((1*S*,2*S*)-2-((fluoromethoxy)methyl)cyclopropyl)methoxy)-5-(3-**
58 **methoxyazetidino-1-yl)picolinamido)butanoate (8)**
59
60

¹H NMR (600 MHz, DMSO-*d*₆) δ 8.39 (s, 1H), 7.47 (d, *J* = 7.9 Hz, 1H), 6.73 (d, *J* = 7.9 Hz, 1H), 5.30 (d, *J* = 56.8 Hz, 2H), 4.32 – 4.15 (m, 7H), 3.82 – 3.77 (m, 2H), 3.67 – 3.59 (m, 1H), 3.58 – 3.50 (m, 1H), 3.24 (s, 3H), 2.39 – 2.34 (m, 2H), 1.84 – 1.77 (m, 2H), 1.31 – 1.22 (m, 5H), 0.72 – 0.57 (m, 8H). LC-MS (ESI): 481.2609 [M+H⁺]; calculated for C₂₄H₃₅FN₃O₆+H⁺: 481.2588.

Fluoromethyl 2-ethyl-2-(6-(((1*S*,2*S*)-2-(hydroxymethyl)cyclopropyl)methoxy)-5-(3-methoxyazetid-1-yl)picolinamido)butanoate (9)

¹H NMR (600 MHz, Chloroform-*d*) δ 8.55 (s, 1H), 7.63 (d, *J* = 7.9 Hz, 1H), 6.60 (d, *J* = 7.9 Hz, 1H), 5.81 (ddd, *J* = 56.8, 9.0, 1.9 Hz, 2H), 4.52 – 4.43 (m, 1H), 4.33 – 4.26 (m, 3H), 4.12 – 4.06 (m, 1H), 3.90 – 3.85 (m, 2H), 3.66 – 3.61 (m, 1H), 3.40 – 3.35 (m, 1H), 3.34 (s, 3H), 2.66 – 2.58 (m, 2H), 1.97 – 1.90 (m, 2H), 1.39 – 1.34 (m, 1H), 1.23 – 1.19 (m, 1H), 0.84 – 0.78 (m, 6H), 0.70 – 0.67 (m, 1H), 0.59 – 0.56 (m, 1H) (OH not visible). LC-MS (ESI): 453.2282 [M+H⁺]; calculated for C₂₂H₃₁FN₃O₆+H⁺: 453.2275.

2-Fluoroethyl 2-ethyl-2-(6-(((1*S*,2*S*)-2-(hydroxymethyl)cyclopropyl)methoxy)-5-(3-methoxyazetid-1-yl)picolinamido)butanoate (10)

¹H NMR (600 MHz, Chloroform-*d*) δ 8.70 (s, 1H), 7.64 (d, *J* = 7.9 Hz, 1H), 6.61 (d, *J* = 7.9 Hz, 1H), 4.70 – 4.65 (m, 2H), 4.62 – 4.59 (m, 1H), 4.46 (dt, *J* = 47.7, 4.1 Hz, 2H), 4.31 – 4.26 (m, 3H), 3.94 – 3.85 (m, 3H), 3.74 – 3.69 (m, 1H), 3.34 (s, 3H), 3.27 – 3.23 (m, 1H), 2.70 – 2.61 (m, 2H), 1.96 – 1.89 (m, 2H), 1.47 – 1.42 (m, 1H), 1.23 – 1.17 (m, 1H), 0.82 – 0.76 (m, 6H), 0.69 – 0.66 (m, 1H), 0.56 – 0.52 (m, 1H) (OH not visible). LC-MS (ESI): 467.2435 [M+H⁺]; calculated for C₂₃H₃₄FN₃O₆+H⁺: 467.2432.

3-Fluoropropyl 2-ethyl-2-(6-(((1*S*,2*S*)-2-(hydroxymethyl)cyclopropyl)methoxy)-5-(3-methoxyazetid-1-yl)picolinamido)butanoate (11, RoSMA-18)

¹H NMR (600 MHz, Chloroform-*d*) δ 8.73 (s, 1H), 7.63 (d, *J* = 7.9 Hz, 1H), 6.61 (d, *J* = 7.9 Hz, 1H), 4.74 – 4.69 (m, 1H), 4.55 (dt, *J* = 47.7, 4.1 Hz, 2H), 4.37 – 4.26 (m, 5H), 3.90 – 3.84 (m, 3H), 3.76 – 3.71 (m, 1H), 3.34 (s, 3H), 3.25 – 3.21 (m, 1H), 2.70 – 2.60 (m, 2H), 2.09 (dq, *J* = 25.6, 5.9 Hz, 2H), 1.90 – 1.82 (m, 2H), 1.49 – 1.45 (m, 1H), 1.22 – 1.18 (m, 1H), 0.81 – 0.74 (m, 6H), 0.69 – 0.65 (m, 1H),

0.56 – 0.52 (m, 1H) (OH not visible). ^{13}C NMR (600 MHz, DMSO- d_6) δ 173.5, 162.8, 151.4, 138.5, 135.0, 118.2, 116.5, 81.1, 70.1, 69.2, 64.8, 63.9, 61.8, 60.2, 55.8, 29.5, 27.8, 19.8, 15.5, 8.6, 8.5. LC-MS (ESI): 481.2596 [M+H $^+$]; calculated for C₂₄H₃₅FN₃O₆+H $^+$: 481.2588.

3-fluoropropyl-1,1,2,2,3,3-d₆ 2-ethyl-2-(6-(((1S,2S)-2-(hydroxymethyl)cyclopropyl)methoxy)-5-(3-methoxyazetid-1-yl)picolinamido)butanoate (11-d₆, RoSMA-18-d₆)

^1H NMR (500 MHz, DMSO- d_6) δ 8.33 (s, 1 H), 7.46 (d, $J = 7.8$ Hz, 1H), 6.72 (d, $J = 7.8$ Hz, 1H), 4.53 (t, $J = 5.5$ Hz, 1H), 4.21 - 4.28 (m, 4H), 4.15 (br d, $J = 7.4$ Hz, 1H), 3.80 (br d, $J = 8.6$ Hz, 2 H), 3.27 - 3.33 (m, 2 H), 3.24 (s, 3 H), 2.28 - 2.36 (m, 2 H), 1.86 - 1.91 (m, 1H), 1.83 (dd, $J = 13.9, 7.3$ Hz, 1H), 1.10 - 1.21 (m, 1H), 0.99 - 1.08 (m, 1H), 0.66 - 0.72 (m, 6H), 0.47 - 0.55 (m, 2H) (OH not visible). ^{13}C NMR (126 MHz, DMSO- d_6) δ 173.7, 163.0, 151.5, 138.7, 135.2, 118.3, 116.6, 70.1, 69.3, 64.9, 64.0, 60.3, 55.9, 27.9, 20.0, 15.6, 8.7, 8.6. LC-MS (ESI): 488.3041 [M+H $^+$]; calculated for C₂₄H₃₀D₆FN₃O₆+H $^+$: 488.3038.

Fluoromethyl 2-ethyl-2-(6-(((1S,2R)-2-(hydroxymethyl)cyclopropyl)methoxy)-5-(3-methoxyazetid-1-yl)picolinamido)butanoate (12)

^1H NMR (600 MHz, DMSO- d_6) δ 8.21 (s, 1H), 7.46 (d, $J = 7.9$ Hz, 1H), 6.72 (d, $J = 7.9$ Hz, 1H), 5.84 (d, $J = 56.8$ Hz, 2H), 4.51 (t, $J = 5.5$ Hz, 1H), 4.29 – 4.22 (m, 4H), 4.17 – 4.12 (m, 1H), 3.82 – 3.78 (m, 2H), 3.24 (s, 3H), 2.39 – 2.21 (m, 2H), 1.97 – 1.88 (m, 2H), 1.18 – 1.12 (m, 1H), 1.06 – 1.01 (m, 1H), 0.74 (t, $J = 7.3$ Hz, 6H), 0.55 – 0.48 (m, 2H) (OH not visible). LC-MS (ESI): 453.2278 [M+H $^+$]; calculated for C₂₂H₃₁FN₃O₆+H $^+$: 453.2275.

2-Fluoroethyl 2-ethyl-2-(6-(((1S,2R)-2-(hydroxymethyl)cyclopropyl)methoxy)-5-(3-methoxyazetid-1-yl)picolinamido)butanoate (13)

^1H NMR (600 MHz, Chloroform- d) δ 8.70 (s, 1H), 7.63 (d, $J = 7.9, 1.4$ Hz, 1H), 6.60 (d, $J = 7.9$ Hz, 1H), 4.70 – 4.65 (m, 2H), 4.62 – 4.58 (m, 1H), 4.46 (dt, $J = 47.7, 4.1$ Hz, 2H), 4.32 – 4.25 (m, 3H), 3.92 – 3.85 (m, 3H), 3.74 – 3.69 (m, 1H), 3.34 (s, 3H), 3.28 – 3.22 (m, 1H), 2.70 – 2.60 (m, 2H), 1.96 – 1.89

(m, 2H), 1.47 – 1.41 (m, 1H), 1.23 – 1.17 (m, 1H), 0.82 – 0.75 (m, 6H), 0.69 – 0.66 (m, 1H), 0.56 – 0.52 (m, 1H) (OH not visible). LC-MS (ESI): 467.2439 [M+H⁺]; calculated for C₂₃H₃₃FN₃O₆ +H⁺: 467.2432.

3-Fluoropropyl 2-ethyl-2-(6-(((1S,2R)-2-(hydroxymethyl)cyclopropyl)methoxy)-5-(3-methoxyazetid-1-yl)picolinamido)butanoate (14)

¹H NMR (600 MHz, Chloroform-*d*) δ 8.73 (s, 1H), 7.63 (d, *J* = 7.9 Hz, 1H), 6.61 (d, *J* = 7.9 Hz, 1H), 4.74 – 4.69 (m, 1H), 4.55 (dt, *J* = 47.7, 4.1 Hz, 2H), 4.37 – 4.26 (m, 5H), 3.90 – 3.84 (m, 3H), 3.76 – 3.71 (m, 1H), 3.34 (s, 3H), 3.25 – 3.21 (m, 1H), 2.70 – 2.60 (m, 2H), 2.09 (dq, *J* = 25.6, 5.9 Hz, 2H), 1.90 – 1.82 (m, 2H), 1.49 – 1.45 (m, 1H), 1.22 – 1.18 (m, 1H), 0.81 – 0.74 (m, 6H), 0.69 – 0.65 (m, 1H), 0.56 – 0.52 (m, 1H) (OH not visible). LC-MS (ESI): 481.2603 [M+H⁺]; calculated for C₂₄H₃₅FN₃O₆ +H⁺: 481.2588.

Ethyl 2-ethyl-2-(6-(((1R,2R)-2-((fluoromethoxy)methyl)cyclopropyl)methoxy)-5-(3-methoxyazetid-1-yl)picolinamido)butanoate (15)

¹H NMR (600 MHz, DMSO-*d*₆) δ 8.39 (s, 1H), 7.47 (d, *J* = 7.9 Hz, 1H), 6.73 (d, *J* = 7.9 Hz, 1H), 5.30 (d, *J* = 56.8 Hz, 2H), 4.32 – 4.15 (m, 7H), 3.82 – 3.77 (m, 2H), 3.67 – 3.59 (m, 1H), 3.58 – 3.50 (m, 1H), 3.24 (s, 3H), 2.39 – 2.34 (m, 2H), 1.84 – 1.77 (m, 2H), 1.31 – 1.22 (m, 5H), 0.72 – 0.57 (m, 8H). LC-MS (ESI): 481.2605 [M+H⁺]; calculated for C₂₄H₃₅FN₃O₆ +H⁺: 481.2588.

3-(Tosyloxy)propyl-2-ethyl-2-(6-(((1S,2S)-2-(hydroxymethyl)cyclopropyl)methoxy)-5-(3-methoxy-azetid-1-yl)picolinamido)butanoate (precursor):

¹H-NMR (400 MHz, Chloroform-*d*): δ 8.61 (s, 1H), 7.75 (d, *J* = 8.1 Hz, 2H), 7.61-7.55 (m, 1H), 7.31 (d, *J* = 8.1 Hz, 2H), 6.60-6.51 (m, 1H), 4.64-4.54 (m, 1H), 4.30-4.19 (m, 5H), 4.08 (t, *J* = 6.0 Hz, 2H), 3.96-3.77 (m, 3H), 3.71-3.60 (m, 1H), 3.30 (s, 3H), 3.28-2.22 (m, 1H), 2.63-2.45 (m, 2H), 2.41 (s, 3H), 2.07-1.96 (m, 2H), 1.79-1.65 (m, 2H), 1.45-1.33 (br, 1H), 1.20-1.11 (br, 1H), 0.74-0.60 (m, 7H), 0.57-0.48 (m, 1H), (OH not visible). LC-MS (ESI): 634.2785 [M+H⁺]; calculated for C₂₄H₃₅FN₃O₆ + H⁺: 634.2793.

3-(Tosyloxy)propyl-1,1,2,2,3,3-*d*₆-2-ethyl-2-(6-(((1*S*,2*S*)-2-(hydroxymethyl)cyclopropyl)methoxy)-5-(3-methoxyazetididin-1-yl)picolinamido)butanoate (precursor-*d*₆):

¹H-NMR (400 MHz, Chloroform-*d*): δ 8.61 (s, 1H), 7.75 (d, *J* = 8.1 Hz, 2H), 7.61-7.55 (m, 1H), 7.31 (d, *J* = 8.1 Hz, 2H), 6.60-6.51 (m, 1H), 4.64-4.54 (m, 1H), 4.36-4.22 (m, 3H), 3.96-3.77 (m, 3H), 3.71-3.60 (m, 1H), 3.30 (s, 3H), 3.28-2.22 (m, 1H), 2.63-2.45 (m, 2H), 2.41 (s, 3H), 1.79-1.65 (m, 2H), 1.45-1.33 (br, 1H), 1.20-1.11 (br, 1H), 0.74-0.60 (m, 7H), 0.57-0.48 (m, 1H), (OH not visible). LC-MS (ESI): 662.2979 [M+Na⁺]; calculated for C₂₄H₃₅FN₃O₆+Na⁺: 662.2989.

Ethyl 2-(6-(((*cis*)-2-(((*tert*-butyldimethylsilyl)oxy)methyl)cyclopropyl)methoxy)-5-(3-methoxyazetididin-1-yl)picolinamido)-2-ethylbutanoate (I)

¹H NMR (300 MHz, DMSO-*d*₆) δ 8.38 (s, 1H), 7.46 (d, *J* = 7.9 Hz, 1H), 6.72 (d, *J* = 7.9 Hz, 1H), 4.46 (dd, *J* = 11.4, 7.9 Hz, 1H), 4.34 (dd, *J* = 11.4, 7.9 Hz, 1H), 4.32 (m, 1H), 4.27 (t, d, *J* = 7.9 Hz, 4H), 3.86 – 3.64 (m, 4H), 3.29 (s, 3H), 2.37 (m, 2H), 1.80 (dq, *J* = 14.5, 7.3 Hz, 2H), 1.48 – 1.32 (m, 1H), 1.26 – 1.12 (m, 1H), 1.20 (t, *J* = 7.1 Hz, 3H), 0.82 – 0.75 (dd, *J* = 5.4, 5.4 Hz, 1H), 0.82 (s, 9H), 0.68 (t, *J* = 7.4 Hz, 6H), 0.38 (dd, *J* = 5.4, 5.4 Hz, 1H), -0.03 (d, *J* = 1.2 Hz, 6H). LC-MS (ESI): 564.3469 [M+H⁺]; calculated for C₂₉H₄₉N₃O₆Si + H⁺: 564.3467.

Ethyl 2-ethyl-2-(6-(((*cis*)-2-(hydroxymethyl)cyclopropyl)methoxy)-5-(3-methoxyazetididin-1-yl)picolinamido)butanoate (II)

¹H NMR (300 MHz, DMSO-*d*₆) δ 8.38 (s, 1H), 7.47 (d, *J* = 7.8 Hz, 1H), 6.72 (d, *J* = 7.8 Hz, 1H), 4.56 (dd, *J* = 11.5, 7.1 Hz, 1H), 4.45 (t, *J* = 5.2 Hz, 1H), 4.36 – 4.14 (m, 6H), 3.79 (dd, *J* = 8.1, 3.5 Hz, 1H), 3.52 (td, *J* = 7.1, 5.1 Hz, 2H), 3.24 (s, 3H), 2.36 (ddd, *J* = 13.7, 7.3, 2.3 Hz, 2H), 1.81 (dq, *J* = 14.5, 7.3 Hz, 2H), 1.46 – 1.29 (m, 1H), 1.23 (t, *J* = 6.1 Hz, 3H), 1.17 (t, *J* = 6.1 Hz, 3H), 0.76 (td, *J* = 8.5, 4.6 Hz, 1H), 0.73 – 0.68 (m, 1H), 0.68 (t, *J* = 7.5 Hz, 3H), 0.33 (q, *J* = 5.3 Hz, 1H). LCMS (ESI): 450.3 [M+H⁺].

Ethyl 2-(5-bromo-6-(((1*R*,2*S*)-2-(((*tert*-butyldimethylsilyl)oxy)methyl)cyclopropyl)methoxy)picolinamido)-2-ethylbutanoate (IV)

¹H NMR (300 MHz, DMSO-*d*₆) δ 8.60 (s, 1H), 8.22 (d, *J* = 7.8 Hz, 1H), 7.51 (d, *J* = 7.8 Hz, 1H), 4.62 (dd, *J* = 11.4, 7.5 Hz, 1H), 4.44 (dd, *J* = 11.4, 7.5 Hz, 1H), 4.24 (q, *J* = 7.1 Hz, 2H), 3.82 (dd, *J* = 11.1, 6.5 Hz, 1H), 3.72 (dd, *J* = 11.1, 6.5 Hz, 1H), 2.46 – 2.25 (m, 2H), 1.84 (dq, *J* = 14.6, 7.4 Hz, 2H), 1.44 (dd, *J* = 14.3, 7.2 Hz, 1H), 1.23 (t, *J* = 7.1 Hz, 4H), 0.84 (dd, *J* = 8.5, 4.7 Hz, 1H), 0.80 (m, 1H), 0.79 (s, 9H), 0.70 (td, *J* = 7.3, 1.1 Hz, 6H), 0.46 (q, *J* = 5.4 Hz, 1H), -0.03 (d, *J* = 1.2 Hz, 6H). LC-MS (ESI): 559.2032 [M+H⁺]; calculated for C₂₅H₄₁BrN₂O₅Si + H⁺: 559.2046.

6-(3-(Benzyloxy)-2,2-dimethylpropoxy)-5-bromopicolinic acid (VII)

¹H NMR (600 MHz, DMSO-*d*₆) δ 13.28 (s, 1H), 8.17 (d, *J* = 7.8 Hz, 1H), 7.56 (d, *J* = 7.8 Hz, 1H), 7.35 – 7.18 (m, 5H), 4.46 (s, 2H), 4.19 (s, 2H), 3.34 (s, 2H), 1.03 (s, 6H). LC-MS (ESI): 394.0666 [M+H⁺]; calculated for C₁₈H₂₀BrNO₄ + H⁺: 394.0655.

Ethyl 2-(6-(3-(benzyloxy)-2,2-dimethylpropoxy)-5-bromopicolinamido)-2-ethylbutanoate (VIII)

¹H NMR (600 MHz, DMSO-*d*₆) δ 8.66 (s, 1H), 8.21 (d, *J* = 7.8 Hz, 1H), 7.53 (d, *J* = 7.8 Hz, 1H), 7.29 – 7.18 (m, 5H), 4.46 (s, 2H), 4.26 (s, 2H), 4.23 (q, *J* = 7.1 Hz, 2H), 3.36 (s, 2H), 2.38 (dq, *J* = 13.7, 7.5 Hz, 2H), 1.84 (dq, *J* = 13.7, 7.5 Hz, 2H), 1.23 (t, *J* = 7.1 Hz, 3H), 1.04 (s, 6H), 0.71 (t, *J* = 7.5 Hz, 6H). LC-MS (ESI): 537.1814 [M+H⁺]; calculated for C₁₂₆H₃₅BrN₂O₅ + H⁺: 537.1826.

Ethyl 2-(6-(3-(benzyloxy)-2,2-dimethylpropoxy)-5-(3-methoxyazetidino-1-yl)picolinamido)-2-ethylbutanoate (X)

¹H NMR (300 MHz, DMSO-*d*₆) δ 8.45 (s, 1H), 7.48 (d, *J* = 7.8 Hz, 1H), 7.29 – 7.18 (m, 5H), 6.70 (d, *J* = 7.8 Hz, 1H), 4.48 (s, 2H), 4.28 – 4.09 (m, 7H), 3.72 (dd, *J* = 9.1, 3.9 Hz, 2H), 3.32 (s, 2H), 3.24 (s, 3H), 2.39 (dq, *J* = 14.7, 7.4 Hz, 2H), 1.80 (dq, *J* = 14.7, 7.4 Hz, 2H), 1.25 – 1.19 (m, 3H), 1.04 (s, 6H), 0.69 (t, *J* = 7.4 Hz, 6H). LC-MS (ESI): 542.3246 [M+H⁺]; calculated for C₃₀H₄₃N₃O₆ + H⁺: 542.3242.

Ethyl 2-ethyl-2-(6-(3-hydroxy-2,2-dimethylpropoxy)-5-(3-methoxyazetidino-1-yl)picolinamido)butanoate (XI)

¹H NMR (600 MHz, DMSO-*d*₆) δ 8.44 (s, 1H), 7.47 (d, *J* = 7.9 Hz, 1H), 6.71 (d, *J* = 7.9 Hz, 1H), 4.69 – 4.64 (m, 1H), 4.36 – 4.14 (m, 5H), 4.10 (s, 2H), 3.87 – 3.75 (m, 2H), 3.37 – 3.28 (m, 2H), 3.25 (s, 3H), 2.50 – 2.27 (dq, *J* = 14.4, 7.3 Hz, 2H), 1.80 (dq, *J* = 14.4, 7.3 Hz, 2H), 1.23 (t, *J* = 7.1 Hz, 3H), 0.95 (s, 6H), 0.70 (t, *J* = 7.4 Hz, 6H). LC-MS (ESI): 452.2779 [M+H⁺]; calculated for C₂₃H₃₇N₃O₆ + H⁺: 452.2775.

6-(((*trans*)-2-((benzyloxy)methyl)cyclopropyl)methoxy)-5-bromopicolinic acid (XII)

¹H NMR (600 MHz, DMSO-*d*₆) δ 13.25 (s, 1H), 8.17 (d, *J* = 7.8 Hz, 1H), 7.54 (d, *J* = 7.8 Hz, 1H), 7.35 – 7.29 (m, 2H), 7.29 – 7.23 (m, 3H), 4.47 (q, *J* = 12.2 Hz, 2H), 4.34 (dd, *J* = 11.3, 6.6 Hz, 1H), 4.28 (dd, *J* = 11.3, 7.1 Hz, 1H), 3.45 (dd, *J* = 10.6, 5.9 Hz, 1H), 3.24 (dd, *J* = 10.6, 7.0 Hz, 1H), 1.27 – 1.18 (m, 2H), 0.65 (dt, *J* = 8.2, 4.9 Hz, 1H), 0.51 (dt, *J* = 8.2, 4.9 Hz, 1H). LC-MS (ESI): 392.0501 [M+H⁺]; calculated for C₁₈H₁₈BrNO₄ + H⁺: 392.0501.

Ethyl 2-(6-(((*trans*)-2-((benzyloxy)methyl)cyclopropyl)methoxy)-5-bromopicolinamido)-2-ethylbutanoate (XIII)

¹H NMR (600 MHz, DMSO-*d*₆) δ 8.62 (s, 1H), 8.21 (d, *J* = 7.9 Hz, 1H), 7.51 (d, *J* = 7.9 Hz, 1H), 7.36 – 7.28 (m, 2H), 7.28 – 7.23 (m, 3H), 4.51 – 4.37 (m, 4H), 4.22 (q, *J* = 7.1 Hz, 2H), 3.41 (dd, *J* = 10.6, 6.2 Hz, 1H), 3.26 (dd, *J* = 10.6, 7.1 Hz, 1H), 2.36 (dq, *J* = 14.9, 7.3 Hz, 2H), 1.91 – 1.76 (dq, *J* = 14.9, 7.3 Hz, 2H), 1.32 – 1.27 (m, 1H), 1.25 – 1.22 (m, 1H), 1.22 (t, *J* = 7.1 Hz, 3H), 0.70 (t, *J* = 7.3 Hz, 6H), 0.69 (dt, *J* = 8.3, 4.9 Hz, 1H), 0.55 (dt, *J* = 8.3, 4.9 Hz, 1H). LC-MS (ESI): 535.1646 [M+H⁺]; calculated for C₂₆H₃₃BrN₂O₅ + H⁺: 535.1659.

Ethyl 2-(6-(((*trans*)-2-((benzyloxy)methyl)cyclopropyl)methoxy)-5-(3-methoxyazetidino-1-yl)picolinamido)-2-ethylbutanoate (XV)

¹H NMR (600 MHz, DMSO-*d*₆) δ 8.41 (s, 1H), 7.47 (d, *J* = 7.8 Hz, 1H), 7.38 – 7.22 (m, 5H), 6.71 (d, *J* = 7.8 Hz, 1H), 4.44 (s, 2H), 4.36 (dd, *J* = 10.4, 6.4 Hz, 1H), 4.26 – 4.08 (m, 6H), 3.79 – 3.74 (m, 2H), 3.42 (dd, *J* = 10.4, 6.0 Hz, 1H), 3.25 (dd, *J* = 10.4, 7.0 Hz, 1H), 3.20 (s, 3H), 2.37 (dq, *J* = 14.4, 7.4 Hz,

2H), 1.80 (dq, $J = 14.4, 7.4$ Hz, 2H), 1.26 – 1.18 (m, 5H), 0.75 – 0.58 (m, 7H), 0.57 – 0.51 (m, 1H). LC-MS (ESI): 540.3074 [M+H⁺]; calculated for C₃₀H₄₁N₃O₆ + H⁺: 540.3068.

Ethyl 2-ethyl-2-(6-(((*trans*)-2-(hydroxymethyl)cyclopropyl)methoxy)-5-(3-methoxyazetidino-1-yl)picolinamido)butanoate (XVI)

¹H NMR (600 MHz, DMSO) δ 8.40 (s, 1H), 7.46 (d, $J = 7.8$ Hz, 1H), 6.72 (d, $J = 7.8$ Hz, 1H), 4.50 (t, $J = 5.5$ Hz, 1H), 4.29 – 4.20 (m, 6H), 4.15 (dd, $J = 11.1, 7.2$ Hz, 1H), 3.80 (dt, $J = 8.3, 3.7$ Hz, 2H), 2.37 (dq, $J = 14.9, 7.4$ Hz, 2H), 1.80 (dq, $J = 14.5, 7.4$ Hz, 2H), 1.20 – 1.12 (m, 2H), 1.03 (dddd, $J = 11.9, 10.4, 8.3, 4.8$ Hz, 1H), 0.69 (t, $J = 7.4$ Hz, 6H), 0.53 (dt, $J = 8.7, 4.7$ Hz, 1H), 0.50 (dt, $J = 8.3, 4.9$ Hz, 1H). LC-MS (ESI): 450.2640 [M+H⁺]; calculated for C₂₃H₃₅N₃O₆ + H⁺: 450.2560.

2-Ethyl-2-(6-(((1*S*,2*S*)-2-(hydroxymethyl)cyclopropyl)methoxy)-5-(3-methoxyazetidino-1-yl)picolinamido)butanoic acid (XVIII)

¹H NMR (600 MHz, DMSO-*d*₆) δ 13.27 (s, 1H), 8.53 (s, 1H), 7.45 (d, $J = 7.8$ Hz, 1H), 6.72 (d, $J = 7.8$ Hz, 1H), 4.49 (s, 1H), 4.31 – 4.20 (m, 4H), 4.16 (dd, $J = 11.2, 7.2$ Hz, 1H), 3.79 (dt, $J = 8.7, 3.4$ Hz, 2H), 3.30 (d, $J = 6.3$ Hz, 2H), 3.24 (s, 3H), 2.44 – 2.35 (m, 2H), 1.76 (dq, $J = 14.4, 7.3$ Hz, 2H), 1.19 – 1.14 (m, 1H), 1.05 – 0.99 (m, 1H), 0.69 (t, $J = 7.4$ Hz, 6H), 0.53 (dt, $J = 8.3, 4.8$ Hz, 1H), 0.48 (dt, $J = 8.3, 4.8$ Hz, 1H). LC-MS (ESI): 422.2303 [M+H⁺]; calculated for C₂₁H₃₁N₃O₆ + H⁺: 422.2300.

Ethyl 2-ethyl-2-(6-(((1*R*,2*R*)-2-(hydroxymethyl)cyclopropyl)methoxy)-5-(3-methoxyazetidino-1-yl)picolinamido)butanoate (XIX)

¹H NMR (600 MHz, DMSO *d*₆) δ 8.40 (s, 1H), 7.46 (d, $J = 7.8$ Hz, 1H), 6.72 (d, $J = 7.8$ Hz, 1H), 4.50 (t, $J = 5.5$ Hz, 1H), 4.30 – 4.20 (m, 6H), 4.15 (dd, $J = 11.1, 7.2$ Hz, 1H), 3.79 (dt, $J = 8.7, 3.4$ Hz, 2H), 3.24 (s, 3H), 2.38 (dq, $J = 14.5, 6.8$ Hz, 2H), 1.80 (dq, $J = 14.5, 7.3$ Hz, 2H), 1.23 (t, $J = 7.1$ Hz, 3H), 1.17 – 1.12 (m, 1H), 1.03 (dddd, $J = 11.9, 10.4, 8.3, 4.8$ Hz, 1H), 0.69 (t, $J = 7.4$ Hz, 6H), 0.54 (dt, $J = 8.3, 4.8$ Hz, 1H), 0.47 (dt, $J = 8.3, 4.8$ Hz, 1H). LC-MS (ESI): 450.2618 [M+H⁺]; calculated for C₂₃H₃₅N₃O₆ + H⁺: 450.2604.

Synthesis of tritiated analogue:

Ethyl 2-((diphenylmethylene)amino)-4-(phenylsulfinyl)-2-(2-(phenylsulfinyl)ethyl)butanoate (XXII)

In a 250 mL round bottom flask **XXI** (1.9 g, 7.17 mmol, 1 equiv.) was dissolved in THF (40 mL). The solution was cooled down to -78 °C and potassium 2-methylpropan-2-olate (2.4 g, 21.5 mmol, 3 equiv.) was added. (Vinylsulfinyl)benzene (3.2 g, 2.8 mL, 21.5 mmol, 3 equiv.) dissolved in THF (5 mL) was added. The reaction mixture was stirred for 20 min at -78 °C, poured onto water (50 mL) and extracted with AcOEt (3 x 50 mL). The combined organic layers were dried over sodium sulfate and concentrated *in vacuo*. The crude material was purified by flash chromatography (SiO₂, 80 g, 20-90% AcOEt in heptane) to give **XXII** (1.63 g, 2.86 mmol, 40%) as a light yellow oil. ¹H NMR (600 MHz, Chloroform-*d*): δ ppm 7.78 (d, *J* = 8.4 Hz, 1H), 7.28 – 7.68 (m, 19 H), 4.17 (ddd, *J* = 12.3, 5.9, 3.5 Hz, 1H), 4.07 (ddd, *J* = 12.3, 5.9, 3.5 Hz, 1H), 3.54 – 3.59 (m, 2 H), 3.16 – 3.24 (m, 2H), 2.83 – 2.89 (m, 2H), 1.16 – 1.27 (m, 3H). LC-MS (ESI): 572.1903 [M+H⁺]; calculated: 572.1855.

Ethyl 2-((diphenylmethylene)amino)-2-vinylbut-3-enoate (XXIII)

In a 50 mL round bottom flask **XXII** (1.50 g, 2.62 mmol, 1 equiv.) was dissolved in xylene (20 mL). The reaction mixture was heated to 150 °C for 16 h upon stirring, concentrated *in vacuo* poured onto water (50 mL) and extracted with AcOEt (2 x 100 mL). The combined organic layers were dried over sodium sulfate and concentrated *in vacuo*. The crude material was purified by flash chromatography (SiO₂, 40 g, 0-20% AcOEt in heptane) to give **XXIII** (700 mg, 2.19 mmol, 83%) as a light yellow oil. ¹H NMR (600 MHz, Chloroform-*d*): δ ppm 7.28 – 7.68 (m, 10 H), 6.18 (dd, *J* = 15.0, 10.0 Hz, 1H), 5.35 (d, *J* = 15.0 Hz, 1H), 5.18 (d, *J* = 10.0 Hz, 1H), 3.49 – 3.53 (m, 2 H), 1.22 (m, 3 H). LC-MS (ESI): 320.1620 [M+H⁺]; calculated: 320.1650.

2-Amino-2-vinylbut-3-enoate (XXIV)

In a 25 mL round bottom flask **XXIII** (200 mg, 0.63 mmol, 1 equiv.) was dissolved in methanol (5 mL) and water (5 mL). Lithium hydroxide (30 mg, 1.24 mmol, 2 equiv.). The reaction mixture was heated to

1
2
3 90 °C for 2 h upon stirring, poured onto water (10 mL) and AcOEt (10 mL). The aqueous layer was
4 separated and lyophilized to give **XXIV** (80 mg, 0.62 mmol, 96%) as a white solid. ¹H NMR (600 MHz,
5 DMSO *d*₆) δ 8.94 (s, 2H), 6.07 (dd, *J* = 17.5, 10.9 Hz, 2H), 5.50 (d, *J* = 10.9 Hz, 2H), 5.44 (d, *J* = 17.5
6 Hz, 2H). LC-MS (ESI): 128.0704 [M+H⁺]; calculated: 128.0702.
7
8
9
10

11 12 **3-Fluoropropyl 2-amino-2-vinylbut-3-enoate (XXV)**

13
14
15 In a 10 mL round bottom flask **XXIV** (0.18 g, 1.1 mmol, 1 equiv.) was dissolved in 3-fluoropropan-1-
16 ol (1.55 g, 1.6 mL, 19.8 mmol, 18 equiv.). Thionyl chloride (1.31 g, 800 μL, 11 mmol, 10 eq) was added
17 at 0 °C. The reaction mixture was heated to 80 °C upon stirring for 1 h, poured onto water (10 mL) and
18 extracted with CH₂Cl₂ (3 x 50 mL). The combined organic layers were dried over sodium sulfate and
19 concentrated *in vacuo*. The crude material was purified by flash chromatography (SiO₂, 12 g, 20-70%
20 AcOEt in heptane) to give the **XXV** (0.21 g, 539 μmol, 49%) as a colourless oil. ¹H NMR (600 MHz,
21 Chloroform-*d*) δ 6.11 (dd, *J* = 17.3, 10.5 Hz, 2H), 5.37 (dd, *J* = 17.3, 0.7 Hz, 2H), 5.21 (dd, *J* = 10.5,
22 0.7 Hz, 2H), 4.56 (t, *J* = 5.8 Hz, 1H), 4.48 (t, *J* = 5.8 Hz, 1H), 4.29 (t, *J* = 6.3 Hz, 2H), 2.07 (qd, *J* = 6.3,
23 5.8 Hz, 1H), 2.03 (qd, *J* = 6.3, 5.7 Hz, 1H). LC-MS (ESI): 188.1082 [M+H⁺]; calculated: 188.1079.
24
25
26
27
28
29
30
31
32
33
34

35 **6-(((1S,2S)-2-(Hydroxymethyl)cyclopropyl)methoxy)-5-(3-methoxyazetidino-1-yl)picolinamide** 36 37 **(XXVI)**

38
39
40 In a 30 mL round bottom flask **XVIII** (0.34 g, 0.80 mmol, 1.0 equiv.) was dissolved in Toluene (14
41 mL). Triethylamine (81.0 mg, 116 μL, 0.80 mmol, 1.0 equiv.) and DPPA (221 mg, 173 μL, 0.80 μmol,
42 1.0 equiv.) were added and the reaction mixture was stirred for 24 h at rt. The reaction mixture was
43 poured onto water (20 mL) and extracted with AcOEt (3 x 30 mL). The combined organic layers were
44 dried over sodium sulfate and concentrated *in vacuo*. The obtained white solid was dissolved toluene
45 (10.0 mL), heated to 110 °C upon stirring for 3 h and then concentrated *in vacuo*. The crude material
46 was purified by flash chromatography (SiO₂, 120 g, 10-70% AcOEt in heptane) to give **XXVI** (120 mg,
47 0.40 mmol, 48%) as a off white solid. ¹H NMR (600 MHz, Chloroform-*d*): δ ppm 8.18 (s, 2H), 7.74 (d,
48 *J* = 8.0 Hz, 1H), 6.56 (d, *J* = 8.0 Hz, 1H), 3.99 - 4.41 (m, 7 H), 3.95 - 4.00 (m, 2 H), 3.32 - 3.27 (m, 3
49 H), 1.20 - 1.36 (m, 2H), 0.54 - 0.79 (m, 2 H). LC-MS (ESI): 308.1702 [M+H⁺]; calculated: 308.1610.
50
51
52
53
54
55
56
57
58
59
60

1
2
3 **6-(((1S,2S)-2-(Hydroxymethyl)cyclopropyl)methoxy)-5-(3-methoxyazetidino-1-yl)picolinic acid**
4
5 **(XXVII)**
6
7

8 In a 25 mL round bottom flask **XXVI** (85.0 mg, 0.28 mmol, 1.0 equiv.) was dissolved in Methanol (3.0
9 mL) and Water (5.0 mL). Sodium hydroxide (55.0 mg, 1.38 mmol, 5 equiv.) was added and the reaction
10 mixture was heated to 85 °C upon stirring for 12 h, poured onto water (10 mL) and 1N HCl (3.0 mL),
11 and extracted with AcOEt (3 x 20 mL). The combined organic layers were dried over sodium sulfate
12 and concentrated *in vacuo*. The crude material was purified by flash chromatography (SiO₂, 12 g, 40-
13 100% AcOEt in heptane) to give **XXVII** (64.0 mg, 0.21 mmol, 75%) as an off white solid. ¹H NMR
14 (600 MHz, Chloroform-*d*): δ ppm 7.72 (dd, *J* = 7.9, 2.9 Hz, 1 H), 6.56 (d, *J* = 7.9 Hz, 1 H), 3.99 - 4.41
15 (m, 7H), 3.97 - 3.99 (m, 2 H), 3.28 (m, 3 H), 1.18 - 1.32 (m, 2H), 0.56 - 0.81 (m, 2 H). LC-MS (ESI):
16 309.1451 [M+H⁺]; calculated: 309.1379.
17
18
19
20
21
22
23
24
25
26
27

28 **3-Fluoropropyl 2-(6-(((1S,2S)-2-(hydroxymethyl)cyclopropyl)methoxy)-5-(3-methoxyazetidino-1-**
29 **yl)picolinamido)-2-vinylbut-3-enoate ([³H]RoSMA-18-Precursor)**
30
31
32

33 In a 10 mL round bottom flask **XXVII** (20 mg, 64 μmol, 0.8 equiv.) was dissolved in CH₂Cl₂ (2 mL).
34 **XXV** (15 mg, 80 μmol, 1 equiv.), HATU (37 mg, 96 μmol, 1.2 equiv.) and DIPEA (41 mg, 55 μL, 320
35 μmol, 4 equiv.) were added. The reaction mixture was stirred for 4 h at ambient temperature, poured
36 onto water (10 mL) and extracted with AcOEt (3 x 15 mL). The combined organic layers were dried
37 over sodium sulfate and concentrated *in vacuo*. The crude material was purified by flash
38 chromatography (SiO₂, 40 g, 20 - 70% AcOEt in heptane) to give [³H]RoSMA-18-Precursor (13 mg,
39 32 μmol, 34%) as a colourless oil. ¹H NMR (600 MHz, Chloroform-*d*): δ 8.46 (s, 1H), 7.65 (d, *J* = 7.8
40 Hz, 1H), 6.58 (d, *J* = 7.9 Hz, 1H), 6.26 (ddd, *J* = 17.2, 10.5, 1.2 Hz, 2H), 5.36 - 5.31 (m, 4H), 4.53 (t, *J*
41 = 5.8 Hz, 1H), 4.45 (t, *J* = 5.8 Hz, 1H), 4.38 (dd, *J* = 11.2, 6.7 Hz, 1H), 4.33 (t, *J* = 6.2 Hz, 2H), 4.32 -
42 4.26 (m, 3H), 4.15 - 4.11 (m, 2H), 3.88 (qd, *J* = 4.7, 2.8 Hz, 2H), 3.64 (dd, *J* = 11.3, 6.3 Hz, 1H), 3.41
43 (dd, *J* = 11.3, 7.5 Hz, 1H), 1.99 - 2.10 (m, 2H), 1.53 - 1.43 (m, 1H), 1.37 - 1.31 (m, 1H), 1.22 - 1.16
44 (m, 1H), 0.67 (dt, *J* = 8.4, 5.0 Hz, 1H), 0.60 (dt, *J* = 8.4, 5.0 Hz, 1H). ¹³C NMR (151 MHz, Chloroform-
45 *d*) δ = 163.56, 151.56, 135.71, 135.60, 117.83, 117.29, 116.63, 116.62, 81.01, 70.25, 69.34, 66.28, 64.70,
46
47
48
49
50
51
52
53
54
55
56
57
58
59
60

1
2
3 62.00, 60.42, 60.19, 56.22, 29.69,16.13, 14.23, 8.56 LC-MS (ESI): 478.2337 [M+H⁺]; calculated:
4
5 478.2334.
6
7

8 **Tritium radiochemistry: Synthesis of [³H]RoSMA-18**

9
10
11 A 2 mL tritiation flask was filled with palladium on charcoal 10% (0.9 mg, 0.8 μmol, 0.2 equiv.) and 3-
12 fluoropropyl [³H]RoSMA-18-precursor (2.0 mg, 4.2 μmol, 1 equiv.) in DMF (0.4 ml). The flask
13 containing this black suspension was attached to an RC Tritec tritium manifold and degassed by three
14 freeze-thaw cycles. Tritium gas was introduced, and the suspension was vigorously stirred for 3 h under
15 an atmosphere of tritium gas at 560 mbar. The suspension was cooled by liquid nitrogen and the excess
16 tritium gas in the reaction vessel was reabsorbed on an uranium trap for waste-tritium. The solvent was
17 lyophilized off, and labile tritium was removed by lyophilization with MeOH (3 × 0.5 mL). The
18 remaining black residue was suspended in ethanol (10 ml) and filtered over a 17 mm Titan HPLC filter
19 (0.45 μm, PTFE) to provide 8.21 GBq (222 mCi) of a crude product in a radiochemical purity of >90%.
20 The crude product was concentrated and purified by preparative HPLC (SunFire C18, 5 μm, 4.6 x 250
21 mm) using acetonitrile [A] and 5% acetonitrile in water [B] as eluent (gradient: 10% [A], 90%[B] to
22 99%[A], 1%[B] in 12 min, hold for 3 min, then back to initial conditions for 5 min, detection at 222 nm,
23 oven temperature at 40°C at a flow rate of 1 mL/min). The combined pure HPLC fractions were
24 concentrated and the product was dissolved and stored in EtOH (50 ml). An amount of 4.59 GBq (124
25 mCi) of [³H]RoSMA-18 was obtained with a radiochemical purity of 98.5% and a molar activity of
26 4.17 TBq/ mmol (113 Ci/mmol), determined by MS spectrometry. The identity of the labeled compound
27 was confirmed by MS and by co-injection of the cold reference standard with the radiolabeled material.
28
29
30
31
32
33
34
35
36
37
38
39
40
41
42
43
44
45
46
47
48

49 **Fluorine-18 radiochemistry: Synthesis of [¹⁸F]RoSMA-18 and [¹⁸F]RoSMA-18-d₆**

50
51
52 [¹⁸F]fluoride was obtained *via* bombardment of 98 % enriched ¹⁸O-water according to the nuclear
53 reaction of ¹⁸O(p,n)¹⁸F in a Cyclone 18/9 cyclotron (18-MeV; IBA Belgium). [¹⁸F]fluoride was trapped
54 on an anion exchange cartridge (Waters SepPak Accell QMA cartridge carbonate), followed by elution
55 with a solution of K₂CO₃ (1 mg/mL) and Krypofix₂₂₂ (2.5 mg/mL) in water/MeCN 1:3. Volatiles were
56 removed at 110 °C under reduced pressure and with a moderate flow of nitrogen. Drying was carried
57
58
59
60

1
2
3 out by the addition of MeCN and subsequent evaporation (3 x 1 mL). 1mg of deuterated or non-
4 deuterated, dissolved in 1mL of dry MeCN was added and the reaction mixture was stirred at 90 °C for
5 10 min. The reaction mixture was allowed to come to ambient temperature and subsequently diluted
6 with water (2.5 mL). The crude residue was purified by semi-preparative HPLC. The desired product
7 was collected in 30 mL of water and passed through a C18 cartridge (Waters, pre-conditioned with 5
8 mL EtOH and 5 mL water). After washing the cartridge with water (5 mL), the desired product was
9 eluted with 0.5 mL EtOH. The final product was formulated in solution containing 5 % EtOH in water
10 for injection (WFI).
11
12
13
14
15
16
17
18
19
20

21 **Partition coefficient (logD_{7.4})**

22
23
24 The partition coefficient logD_{7.4} was determined as previously reported³³. Briefly, an aliquot of the
25 radioligand containing final formulation was diluted in 1-octanol (0.5 mL) and washed with 0.5 mL of
26 phosphate buffer (0.02 M, pH 7.4). The organic layer was isolated and served as radiotracer stock
27 solution. The radiotracer stock solution (5 -10 µL) was diluted in 1-octanol (0.5 mL) and phosphate
28 buffer (0.02 M, pH 7.4, 0.5 mL). The resulting mixture was shaken for 15 min at ambient temperature
29 in an over-head shaker and subsequently centrifuged (3 min, 5000 rpm). 50 µl of each phase were
30 measured on a γ-counter. The partition coefficient was calculated according to **Equation 1**:
31
32
33
34
35
36
37
38
39

$$40 \log D_{7.4} = \log \frac{\text{counts per min (octanol)}}{\text{counts per min (buffer)}} \quad \text{Equation 1}$$

41
42
43 LogD_{7.4} values of non-radioactive compounds were determined by the previously reported CAMDIS
44 method³⁴. Briefly, octanol and phosphate buffer (25 mM, pH 7.4) were mutually saturated at ambient
45 temperature. Compounds were diluted from a DMSO stock solution in phosphate buffer (final DMSO
46 content 1% v/v) and the resulting solutions of 100 µM concentrations were filtered (Millipore Deepwell
47 Multiscreen Filter plate, MDRLN0419) into a 96-well plate and diluted with 200 µL of phosphate buffer.
48 The second dilution step with phosphate buffer was performed to minimize the risk of delayed drug
49 precipitation during the distribution experiment. Filtrate aliquots of 150 µL were transferred into a
50 Teflon plate covered with DIFI tubes (Weizmann Plastics Technology AG, Rapperswil, Switzerland)
51 pre-coated with octanol. The samples were sealed and allowed to shake at ambient temperature for 16-
52
53
54
55
56
57
58
59
60

1
2
3 22 h. The equilibrium concentrations were subsequently determined by LC-UV/MS in the aqueous
4 phase. Reference samples without octanol were included to obtain the initial aqueous compound
5 concentration. The equilibrium concentration in octanol was calculated by mass balance and $\log D_{7.4}$
6 values were calculated according to **Equation 2**.
7
8
9

$$\log D_{7.4} = \log \frac{(C_{aq}^0 - C_{aq}^{eq}) * V_{aq}}{C_{aq}^{eq} * V_{oct}} \quad \text{Equation 2}$$

10
11
12
13
14
15
16
17 C_{aq}^0 , starting concentration of aqueous phase; C_{aq}^{eq} , equilibrium concentration of aqueous phase; V_{aq} ,
18 volume of aqueous phase; V_{oct} , volume of octanol phase.
19
20
21

22 **Metabolite identification**

23 **Liver microsomes study**

24
25
26
27
28
29 Each test compound (10 μ M; 500 μ L) was incubated at 37 $^{\circ}$ C for 1 hour with human or rat liver
30 microsomes (Wistar Han Rat Liver Microsomes R6000, Human Liver Microsomes Xtreme 200,
31 XenoTech, Kansas US). Human liver microsome incubations were performed with a P450 concentration
32 of 250 nM; all other incubations were performed at the total protein concentration used for human
33 incubations. Aliquots of the incubations were taken at 0, 30 and 60 min, quenched with ice-cold
34 acetonitrile (5 x incubation volume) and centrifuged at 2000g and 4 $^{\circ}$ C for 10 min. Subsequently, the
35 supernatants were reduced to dryness under nitrogen flow at 37 $^{\circ}$ C and analyzed by LC-UV-MS
36 following reconstitution in the initial HPLC mobile phase. Control samples lacking either cofactor
37 NADPH, microsomes or test compound were included in the experiments. Positive controls containing
38 verapamil to ensure appropriate metabolic activity were further conducted. All control samples were
39 analyzed after 60 min incubation according to the procedure described for the test samples.
40
41
42
43
44
45
46
47
48
49
50
51

52
53 The samples were analyzed by UPLC/ToF-MS to monitor metabolite formation, using an LC-MS
54 system (Acquity binary solvent manager, sample manager, column manager and PDA detector from
55 Waters) coupled to a Vion Q-ToF mass spectrometer (Waters). The analytical method was optimized
56 by using the parent compounds for optimum chromatographic properties (peak shape and retention) and
57
58
59
60

1
2
3 mass spectrometric ionization. A range of tools and methodologies were used to detect and identify
4 metabolites, including PDA/MS data comparison with control samples, mass defect filtering, pseudo
5 precursor scanning, full scan MS data acquisition and MSn experiments.
6
7
8

9 10 **Advanced profiling**

11
12
13
14 High throughput solubility assessment by PAMPA, LIMBA and P-gp assays were performed as
15 previously reported by our group^{29, 31, 48, 49}.

16
17
18
19 Briefly, LIMBA was performed by washing Wistar rat whole brains with an aqueous assay buffer
20 containing 50 mM TRIS/114 mM NaCl (pH 7.4), followed by homogenization on ice in 2 volumes (w/v)
21 of n-dodecane⁴⁹. The test compounds were dissolved in DMSO and diluted with the aqueous assay
22 buffer (25 μ M, 0.25% DMSO), which formed the aqueous phase. Incubation was conducted in a sealed
23 kit⁴⁹ at ambient temperature for 15 h. Drug concentrations were measured in the aqueous phase by LC-
24 MS at equilibrium and served to calculate the
25
26
27
28
29
30

31
32
33 LIMBA values by mass balance. All experiments were conducted in triplicates. PAMPA values were
34 obtained by covering a 96-well microtiter plate containing aqueous buffer (0.05 M TRIS, pH 7.4, or
35 0.05 M phosphate, pH 6.5, with a maximum DMSO content of 5%) with a filterplate (“sandwich
36 concept”)⁴⁸. The hydrophobic filter material (Durapore/Millipore; pore size 0.22–0.45 μ m),
37 impregnated with a 1–20% solution of lecithin in an organic solvent (dodecane, hexadecane, 1,9-
38 decadiene), is treated with a small volume (4–5 μ L) of a 50% (v/v) methanol/buffer solution. The actual
39 transport studies were performed by the transfer of 100–200 μ l of a 250 (or 500) μ M stock solution on
40 top of the filterplate in the sample and in the reference section⁴⁸.
41
42
43
44
45
46
47
48

49
50
51 In the P-gp assay, transfected LLC-PK1 cells (porcine kidney epithelial cells, obtained from the
52 Netherlands Cancer Institute) expressing human or mouse P-gp, cultured on a 96-well semi-permeable
53 filter membrane plate were used²⁹. The unidirectional permeability (Papp) of a test compound was
54 measured by separate dosing to the apical (for A>B Papp) and basolateral (for B>A Papp) sides of the
55 monolayer and measuring the movement of the compound into the respective receiver compartments
56 over a 3 h incubation period and at 37 °C²⁹. The P-gp effect was measured by expressing the efflux ratio
57
58
59
60

(ER) of the unidirectional apparent permeability coefficient (Papp) and the mean permeability was assessed in the absence of P-gp by the addition of the selective inhibitor zosuquidar at a concentration of 1 μM ²⁹.

Fluorine-18-based *in vitro* autoradiography

Human and rodent tissue, embedded in TissueTek (O.C.T.), were prepared as sections of 20 μm thickness on a cryostat (Cryo-Star HM 560 MV; Microm, Thermo Scientific, Wilmington, DE, USA) and the slices were adsorbed on SuperFrost Plus (Menzel, Braunschweig, Germany) and subsequently stored at -80 °C till the day of the autoradiographic experiment ²⁹. Slices were thawed and subsequently preconditioned on ice in an incubation buffer (pH 7.4) containing 50 mM TRIS, 5 mM MgCl_2 , 2.5 mM EDTA, and fatty acid free bovine serum albumin (BSA, 5 %). The slices were dried and incubated with the radioligand (dissolved in the incubation buffer) for 15 min at 21 °C in a humidified chamber. For blockade conditions, GW405833 (10 μM) was applied. The slices were washed as follows: 2 x 2 min in a washing buffer (pH 7.4) containing 50 mM TRIS, 5 mM MgCl_2 , 2.5 mM EDTA, 5 % ethanol and fatty acid free bovine serum albumin (BSA, 1 %) and further 2 x 5 s in distilled water. After drying, slices were exposed to a phosphor imager plate (Fuji, Dielsdorf, Switzerland) for 28 min and the film was scanned in a BAS5000 reader (Fuji).

Tritium-based *in vitro* autoradiography

Tissue sections (10 μm) from fresh frozen rat and wt as well as CB2 ko mouse spleen were cut in a cryostat (Leica CM3050) at -17 °C chamber temperature and -15 °C object temperature. Subsequently, tissue sections were thaw-mounted on microscope glass slides (HistoBond, Paul Marienfeld GmbH, Lauda-Königshofen, Germany). Spleen sections were incubated for 30 min in assay buffer (50 mM Tris-HCl, 5 mM MgCl_2 , 2.5 mM EDTA, 5% fatty acid free BSA, pH 7.4) containing the radioligand at 5 nM at room temperature. Non-specific binding was measured using additional sections incubated with assay buffer containing the radiotracer and 10 μM of commercially available CB2 ligand CP55,940. Sections were rinsed three times for 10 min in ice-cold wash buffer (50 mM Tris-HCl, 5 mM MgCl_2 , 2.5 mM EDTA, 1% FAF-BSA pH 7.4) and dipped three times in distilled water at 4 °C. Slide-mounted spleen

1
2
3 sections were dried for at least 3 h and exposed to a Fuji Imaging Plate (BAS-TR 2025, Fujifilm,
4 Dielsdorf, Switzerland) with a [³H]microscale (RPA-510, GE Healthcare, Glattbrugg, Switzerland) for
5 five days. The imaging plate was scanned with 25 μm resolution in a Fujifilm high-resolution plate
6 scanner (BAS-5000, Bucher Biotec AG, Basel, Switzerland). The amount of radioligand bound to the
7 section was measured using the MCID™ image analysis program (version 7; InterFocus Imaging
8 GmbH, Mering, Germany) and expressed as fmol of bound radioligand per mg of protein.
9
10
11
12
13
14
15

16 ***Ex vivo* biodistribution**

17
18
19
20 Biodistribution experiments were carried out with male Wistar rats (n = 4 for each, baseline and blocking
21 conditions). Tracer solution was administered *via* tail-vein injection and the animals were sacrificed 30
22 min post injection. For blocking conditions, commercially available CB2 partial agonist GW-405,833
23 (2 mg/kg) was injected a few seconds before tracer administration. Animals were euthanized by
24 decapitation under isoflurane anesthesia and organs were dissected. Accumulated dose in each organ
25 was measured in a γ-counter and expressed as percent normalized injected dose per gram of organ tissue
26 (norm. % ID/g tissue).
27
28
29
30
31
32
33
34
35

36 **PET experiments**

37
38
39 Small animal PET scans were carried out upon anesthesia with isoflurane (n = 3 for each, baseline and
40 displacement conditions). The radioligand (12 – 17 MBq) was administered *via* tail-vein injection and
41 rodents were scanned for a period of 60 min. Displacement conditions encompassed the injection of 1.5
42 mg/kg of GW-405,833 dissolved in a vehicle of 2% Cremophor (v/v), 10% ethanol (v/v) and 88% aqua
43 ad inject (v/v) at 10 min post radiotracer injection. Control animals were injected with vehicle at 10 min
44 post radiotracer injection. Monitored body temperatures were kept at 37 °C by a heated air stream.
45 Anesthesia depth was measured by respiratory frequency (SA Instruments, Inc., Stony Brook, USA).
46 PET acquisitions were combined with computed tomography (CT) for anatomical orientation and
47 attenuation correction. Data reconstruction was performed in user-defined time frames using a voxel
48 size of 0.3875 x 0.3875 x 0.775 mm³. Images were processed and analyzed using PMOD 3.5 software
49 (PMOD Technologies Ltd., Zurich, Switzerland). The time-activity curves were deduced from specific
50
51
52
53
54
55
56
57
58
59
60

1
2
3 regions of interest (ROIs), that were defined based on a rat MRI T2 template. Radioactivity is presented
4
5 as standardized uptake values (SUV, decay-corrected radioactivity per cm³ divided by the injected dose
6
7 per gram body weight).
8
9

10 ***Ex vivo* metabolite study**

11
12
13
14 *Ex vivo* metabolite experiments were performed with four male Wistar rats (no anesthesia) by
15
16 intravenous injection of the radiotracer (394 – 426 MBq). Plasma samples were harvested at time points
17
18 0, 5, 15, 30 and 45 min and collected in heparin-coated tubes. The plasma was separated from blood
19
20 cells by centrifugation at 5000 g for 5 min (4 °C), subsequent addition of ice-cold MeCN and vortexing,
21
22 followed by a second centrifugation step (5000 g, 5 min, 4 °C). Brain tissue samples were obtained at
23
24 the time points 5 and 45 min and were homogenized in 2mL PBS, combined with 2 mL of MeCN and
25
26 subsequently centrifuged at 5000 g for 5 min (4 °C). Supernatants were analyzed by radio-TLC Instant
27
28 Imager (Packard, Canberra Company, Meriden, Connecticut, USA). The results are given as percentage
29
30 of the total activity.
31
32
33

34 **Associated content**

35 **Supporting information**

36
37
38
39 The Supporting Information is available free of charge on the ACS Publications website.
40
41 Enantioselective precursor syntheses; NMR spectra of target compounds 1 – 15; analytical conditions,
42
43 chromatograms of radiolabeling quality control. Molecular formula strings (CSV)
44
45

46 **Author information**

47 **Corresponding author information**

48
49
50
51 *Email: simon.ametamey@pharma.ethz.ch

52 **ORCID**

53
54
55
56 Ahmed Haider: 0000-0002-5204-4473

57
58 Luca Gobbi: 0000-0002-0563-2491

59
60 Andreas Brink: 0000-0001-6927-8252

1
2
3 Thomas J. Woltering: 0000-0002-5550-1844
4

5 Linjing Mu: 0000-0001-5354-1546
6

7 Uwe Grether: 0000-0002-3164-9270
8

9 Simon M. Ametamey: 0000-0003-4285-6731
10

11 **Abbreviations**

12
13 ALS, Amyotrophic lateral sclerosis; AD, Alzheimer's disease; Ac₂O, acetic anhydride; BINAP, 2,2'-
14 bis(diphenylphosphino)-1,1'-binaphthyl; CB1, Cannabinoid receptor type 1; CB2, Cannabinoid receptor
15 type 2; CT, computed tomography; Chloroform-*d*, deuterated chloroform; CsF, cesium fluoride; DMSO,
16 dimethyl sulfoxide; DIPEA, N,N-Diisopropylethylamine; HCl, hydrochloric acid; KF, potassium
17 fluoride; EOB, end of bombardment; MeCN, acetonitrile; SUV, standardized uptake value; Bq,
18 becquerel; KOAc, potassium acetate; RCY, radiochemical yield; RO, receptor occupancy; EtOAc, ethyl
19 acetate; EtOH, ethanol; NH₄HCO₃, ammonium hydrogen carbonate; H₃PO₄, phosphoric acid; K₂CO₃,
20 potassium carbonate; Hex, hexane; MeOH, methanol; PD, Parkinson's disease; TMS, trimethylamine;
21 NaOH, sodium hydroxide; Pd/C, palladium on carbon; TEA, triethyl amine; Ts, tosylate; K₂C₂O₄,
22 potassium oxalate; WFI, water for injection; HEPES, 4-(2-hydroxyethyl)piperazine-1-ethanesulfonic
23 acid sodium salt; KCl, potassium chloride; MgCl₂, magnesium chloride; OCT, optimal cutting
24 temperature; CaCl₂, calcium chloride; PET, positron emission tomography, TBTU, 2-(1H-
25 Benzotriazole-1-yl)-1,1,3,3-tetramethylaminium tetrafluoro-borate; PDB, protein data bank; TACs,
26 time-activity curves.
27
28
29
30
31
32
33
34
35
36
37
38
39
40
41
42
43
44

45 **Conflict of interest**

46
47
48 The authors declare no conflict of interest.
49

50 **Acknowledgement**

51
52 We thank Bruno Mancosu for his technical assistance with the modules. Markus Margelisch is
53 acknowledged for providing the human spinal cord tissues. We thank Mark Savage for the practical
54 assistance in metabolite identification experiments. We further thank the ALS foundation for partially
55
56
57
58
59
60

1
2
3 funding this project. Isabelle Kaufmann and Fabian Kägi are greatly acknowledged for synthesizing
4 precursors and radiolabeled compounds. We thank Goutam Saha and his colleagues at Chembiotek,
5
6
7 Kolkata, India, for their skilful support in the enantioselective synthesis of chiral intermediate **XIX**.
8
9
10
11
12
13
14
15
16
17
18
19
20
21
22
23
24
25
26
27
28
29
30
31
32
33
34
35
36
37
38
39
40
41
42
43
44
45
46
47
48
49
50
51
52
53
54
55
56
57
58
59
60

References

1. Gaoni, Y.; Mechoulam, R. Isolation, structure, and partial synthesis of an active constituent of hashish. *Journal of the American Chemical Society* **1964**, 86, 1646-1647.
2. Matsuda, L. A.; Lolait, S. J.; Brownstein, M. J.; Young, A. C.; Bonner, T. I. Structure of a cannabinoid receptor and functional expression of the cloned cDNA. *Nature* **1990**, 346, 561-564.
3. Munro, S.; Thomas, K. L.; Abu-Shaar, M. Molecular characterization of a peripheral receptor for cannabinoids. *Nature* **1993**, 365, 61-65.
4. Reggio, P. H. Endocannabinoid binding to the cannabinoid receptors: what is known and what remains unknown. *Current medicinal chemistry* **2010**, 17, 1468-1486.
5. Alpar, A.; Di Marzo, V.; Harkany, T. At the tip of an iceberg: Prenatal marijuana and its possible relation to neuropsychiatric outcome in the offspring. *Biological psychiatry* **2016**, 79, e33-45.
6. Rieder, S. A.; Chauhan, A.; Singh, U.; Nagarkatti, M.; Nagarkatti, P. Cannabinoid-induced apoptosis in immune cells as a pathway to immunosuppression. *Immunobiology* **2010**, 215, 598-605.
7. Gomez, M.; Hernandez, M.; Fernandez-Ruiz, J. Cannabinoid signaling system: does it play a function in cell proliferation and migration, neuritic elongation and guidance and synaptogenesis during brain ontogenesis? *Cell adhesion & migration* **2008**, 2, 246-248.
8. Houser, S. J.; Eads, M.; Embrey, J. P.; Welch, S. P. Dynorphin B and spinal analgesia: induction of antinociception by the cannabinoids CP55,940, Delta(9)-THC and anandamide. *Brain research* **2000**, 857, 337-342.
9. Little, P. J.; Compton, D. R.; Johnson, M. R.; Melvin, L. S.; Martin, B. R. Pharmacology and stereoselectivity of structurally novel cannabinoids in mice. *The Journal of pharmacology and experimental therapeutics* **1988**, 247, 1046-1051.

- 1
2
3 10. Pertwee, R. G.; Ross, R. A. Cannabinoid receptors and their ligands. *Prostaglandins, leukotrienes, and essential fatty acids* **2002**, 66, 101-121.
4
5
6
7
8
9 11. Moreira, F. A.; Grieb, M.; Lutz, B. Central side-effects of therapies based on CB1 cannabinoid
10 receptor agonists and antagonists: focus on anxiety and depression. *Best practice & research. Clinical*
11 *endocrinology & metabolism* **2009**, 23, 133-144.
12
13
14
15 12. Palazuelos, J.; Aguado, T.; Pazos, M. R.; Julien, B.; Carrasco, C.; Resel, E.; Sagredo, O.; Benito,
16 C.; Romero, J.; Azcoitia, I.; Fernandez-Ruiz, J.; Guzman, M.; Galve-Roperh, I. Microglial CB2
17 cannabinoid receptors are neuroprotective in Huntington's disease excitotoxicity. *Brain : a journal of*
18 *neurology* **2009**, 132, 3152-3164.
19
20
21
22
23
24
25 13. Spinelli, F.; Capparelli, E.; Abate, C.; Colabufo, N. A.; Contino, M. Perspectives of cannabinoid
26 type 2 receptor (CB2R) ligands in neurodegenerative disorders: structure–affinity relationship (SAfiR)
27 and structure–activity relationship (SAR) studies. *Journal of Medicinal Chemistry* **2017**, 60, 9913-9931.
28
29
30
31
32
33 14. Dittel, B. N. Direct suppression of autoreactive lymphocytes in the central nervous system via
34 the CB2 receptor. *Br J Pharmacol* **2008**, 153, 271-276.
35
36
37
38 15. Sagredo, O.; Pazos, M. R.; Valdeolivas, S.; Fernandez-Ruiz, J. Cannabinoids: novel medicines
39 for the treatment of Huntington's disease. *Recent patents on CNS drug discovery* **2012**, 7, 41-48.
40
41
42
43 16. Benito, C.; Nunez, E.; Tolon, R. M.; Carrier, E. J.; Rabano, A.; Hillard, C. J.; Romero, J.
44 Cannabinoid CB2 receptors and fatty acid amide hydrolase are selectively overexpressed in neuritic
45 plaque-associated glia in Alzheimer's disease brains. *The Journal of neuroscience : the official journal*
46 *of the Society for Neuroscience* **2003**, 23, 11136-11141.
47
48
49
50
51
52 17. Bie, B.; Wu, J.; Foss, J. F.; Naguib, M. An overview of the cannabinoid type 2 receptor system
53 and its therapeutic potential. *Curr Opin Anaesthesiol* **2018**, 31, 407-414.
54
55
56
57
58
59
60

- 1
2
3 18. Spinelli, F.; Mu, L.; Ametamey, S. M. Radioligands for positron emission tomography imaging
4 of cannabinoid type 2 receptor. *Journal of labelled compounds & radiopharmaceuticals* **2018**, 61, 299-
5 308.
6
7
8
9
10 19. Ahmad, R.; Postnov, A.; Bormans, G.; Versijpt, J.; Vandenbulcke, M.; Van Laere, K. Decreased
11 in vivo availability of the cannabinoid type 2 receptor in Alzheimer's disease. *European journal of*
12 *nuclear medicine and molecular imaging* **2016**, 43, 2219-2227.
13
14
15
16
17 20. Ahmad, R.; Koole, M.; Evens, N.; Serdons, K.; Verbruggen, A.; Bormans, G.; Van Laere, K.
18 Whole-body biodistribution and radiation dosimetry of the cannabinoid type 2 receptor ligand [11C]-
19 NE40 in healthy subjects. *Molecular Imaging and Biology* **2013**, 15, 384-390.
20
21
22
23
24 21. Moldovan, R. P.; Teodoro, R.; Gao, Y.; Deuther-Conrad, W.; Kranz, M.; Wang, Y.; Kuwabara,
25 H.; Nakano, M.; Valentine, H.; Fischer, S.; Pomper, M. G.; Wong, D. F.; Dannals, R. F.; Brust, P.; Horti,
26 A. G. Development of a high-affinity PET radioligand for imaging cannabinoid subtype 2 receptor. *J*
27 *Med Chem* **2016**, 59, 7840-7855.
28
29
30
31
32
33 22. Pottier, G.; Gomez-Vallejo, V.; Padro, D.; Boisgard, R.; Dolle, F.; Llop, J.; Winkeler, A.;
34 Martin, A. PET imaging of cannabinoid type 2 receptors with [(11)C]A-836339 did not evidence
35 changes following neuroinflammation in rats. *Journal of cerebral blood flow and metabolism : official*
36 *journal of the International Society of Cerebral Blood Flow and Metabolism* **2017**, 37, 1163-1178.
37
38
39
40
41
42
43 23. Slavik, R.; Muller Herde, A.; Haider, A.; Kramer, S. D.; Weber, M.; Schibli, R.; Ametamey, S.
44 M.; Mu, L. Discovery of a fluorinated 4-oxo-quinoline derivative as a potential positron emission
45 tomography radiotracer for imaging cannabinoid receptor type 2. *Journal of neurochemistry* **2016**, 138,
46 874-886.
47
48
49
50
51
52 24. Yrjölä, S.; Sarparanta, M.; Airaksinen, A. J.; Hytti, M.; Kauppinen, A.; Pasonen-Seppänen, S.;
53 Adinolfi, B.; Nieri, P.; Manera, C.; Keinänen, O.; Poso, A.; Nevalainen, T. J.; Parkkari, T. Synthesis, in
54 vitro and in vivo evaluation of 1,3,5-triazines as cannabinoid CB2 receptor agonists. *European Journal*
55 *of Pharmaceutical Sciences* **2015**, 67, 85-96.
56
57
58
59
60

- 1
2
3 25. Teodoro, R.; Moldovan, R.-P.; Lueg, C.; Günther, R.; Donat, C. K.; Ludwig, F.-A.; Fischer, S.;
4
5 Deuther-Conrad, W.; Wunsch, B.; Brust, P. Radiofluorination and biological evaluation of N-aryl-
6
7 oxadiazolyl-propionamides as potential radioligands for PET imaging of cannabinoid CB2 receptors.
8
9 *Org Med Chem Lett* **2013**, 3, 11.
10
11
12 26. Ahamed, M.; van Veghel, D.; Ullmer, C.; Van Laere, K.; Verbruggen, A.; Bormans, G. M.
13
14 Synthesis, biodistribution and In vitro evaluation of brain permeable high affinity type 2 cannabinoid
15
16 receptor agonists [(11)C]MA2 and [(18)F]MA3. *Frontiers in neuroscience* **2016**, 10, 431.
17
18
19 27. Haider, A.; Spinelli, F.; Herde, A. M.; Mu, B.; Keller, C.; Margelisch, M.; Weber, M.; Schibli,
20
21 R.; Mu, L.; Ametamey, S. M. Evaluation of 4-oxo-quinoline-based CB2 PET radioligands in R6/2
22
23 chorea huntington mouse model and human ALS spinal cord tissue. *European journal of medicinal*
24
25 *chemistry* **2018**, 145, 746-759.
26
27
28 28. Haider, A.; Muller Herde, A.; Slavik, R.; Weber, M.; Mugnaini, C.; Ligresti, A.; Schibli, R.;
29
30 Mu, L.; Mensah Ametamey, S. Synthesis and biological evaluation of thiophene-based cannabinoid
31
32 receptor type 2 radiotracers for PET imaging. *Frontiers in neuroscience* **2016**, 10, 350.
33
34
35 29. Haider, A.; Kretz, J.; Gobbi, L.; Ahmed, H.; Atz, K.; Bürkler, M.; Bartelmus, C.; Fingerle, J.;
36
37 Guba, W.; Ullmer, C.; Honer, M.; Knuesel, I.; Weber, M.; Brink, A.; Herde, A. M.; Keller, C.; Schibli,
38
39 R.; Mu, L.; Grether, U.; Ametamey, S. M. Structure–activity relationship studies of pyridine-based
40
41 ligands and identification of a fluorinated derivative for positron emission tomography imaging of
42
43 cannabinoid type 2 receptors. *Journal of Medicinal Chemistry* **2019**, 62, 11165-11181.
44
45
46 30. Misumi, A.; Iwanaga, K.; Furuta, K.; Yamamoto, H. Simple asymmetric construction of a
47
48 carbocyclic framework. Direct coupling of dimethyl succinate and 1,omega.-dihalides. *Journal of the*
49
50 *American Chemical Society* **1985**, 107, 3343-3345.
51
52
53 31. Bendels, S.; Bissantz, C.; Fasching, B.; Gerebtzoff, G.; Guba, W.; Kansy, M.; Migeon, J.; Mohr,
54
55 S.; Peters, J. U.; Tillier, F.; Wyler, R.; Lerner, C.; Kramer, C.; Richter, H.; Roberts, S. Safety screening
56
57
58
59
60

1
2
3 in early drug discovery: An optimized assay panel. *Journal of pharmacological and toxicological*
4 *methods* **2019**, *99*, 106609.

5
6
7
8 32. Li, X.; Hua, T.; Vemuri, K.; Ho, J. H.; Wu, Y.; Wu, L.; Popov, P.; Benchama, O.; Zvonok, N.;
9 Locke, K.; Qu, L.; Han, G. W.; Iyer, M. R.; Cinar, R.; Coffey, N. J.; Wang, J.; Wu, M.; Katritch, V.;
10 Zhao, S.; Kunos, G.; Bohn, L. M.; Makriyannis, A.; Stevens, R. C.; Liu, Z. J. Crystal structure of the
11 human cannabinoid receptor CB2. *Cell* **2019**, *176*, 459-467.e13.

12
13
14
15
16
17 33. Wilson, A. A.; Jin, L.; Garcia, A.; DaSilva, J. N.; Houle, S. An admonition when measuring the
18 lipophilicity of radiotracers using counting techniques. *Applied radiation and isotopes : including data,*
19 *instrumentation and methods for use in agriculture, industry and medicine* **2001**, *54*, 203-208.

20
21
22
23
24
25 34. Wagner, B.; Fischer, H.; Kansy, M.; Seelig, A.; Assmus, F. Carrier mediated distribution system
26 (CAMDIS): a new approach for the measurement of octanol/water distribution coefficients. *European*
27 *journal of pharmaceutical sciences : official journal of the European Federation for Pharmaceutical*
28 *Sciences* **2015**, *68*, 68-77.

29
30
31
32
33
34 35. Govaerts, S. J.; Muccioli, G. G.; Hermans, E.; Lambert, D. M. Characterization of the
35 pharmacology of imidazolidinedione derivatives at cannabinoid CB1 and CB2 receptors. *European*
36 *journal of pharmacology* **2004**, *495*, 43-53.

37
38
39
40
41
42 36. Yiangou, Y.; Facer, P.; Durrenberger, P.; Chessell, I. P.; Naylor, A.; Bountra, C.; Banati, R. R.;
43 Anand, P. COX-2, CB2 and P2X7-immunoreactivities are increased in activated microglial
44 cells/macrophages of multiple sclerosis and amyotrophic lateral sclerosis spinal cord. *BMC neurology*
45 **2006**, *6*, 12.

46
47
48
49
50
51 37. Rizzo, M. D.; Henriquez, J. E.; Blevins, L. K.; Bach, A.; Crawford, R. B.; Kaminski, N. E.
52 Targeting cannabinoid receptor 2 on peripheral leukocytes to attenuate inflammatory mechanisms
53 implicated in HIV-associated neurocognitive disorder. *Journal of Neuroimmune Pharmacology* **2020**,
54 doi:10.1007/s11481-020-09918-7

- 1
2
3 38. Piszcz, J. A.; Lemancewicz, D.; Kloczko, J.; Dzieciol, J.; Rusak, M.; Dabrowska, M.
4
5 Cannabinoid receptors expression in bone marrow trephine biopsy of chronic lymphocytic leukaemia
6
7 patients treated with purine analogues. *Experimental oncology* **2007**, *29*, 221-225.
8
9
- 10 39. Staiano, R. I.; Loffredo, S.; Borriello, F.; Iannotti, F. A.; Piscitelli, F.; Orlando, P.; Secondo, A.;
11
12 Granata, F.; Lepore, M. T.; Fiorelli, A.; Varricchi, G.; Santini, M.; Triggiani, M.; Di Marzo, V.; Marone,
13
14 G. Human lung-resident macrophages express CB1 and CB2 receptors whose activation inhibits the
15
16 release of angiogenic and lymphangiogenic factors. *Journal of leukocyte biology* **2016**, *99*, 531-540.
17
18
- 19 40. Giboureau, N.; Emond, P.; Fulton, R. R.; Henderson, D. J.; Chalon, S.; Garreau, L.; Roselt, P.;
20
21 Eberl, S.; Mavel, S.; Bodard, S.; Fulham, M. J.; Guilloteau, D.; Kassiou, M. Ex vivo and in vivo
22
23 evaluation of (2R,3R)-5-[(18)F]-fluoroethoxy- and fluoropropoxy-benzovesamicol, as PET
24
25 radioligands for the vesicular acetylcholine transporter. *Synapse (New York, N.Y.)* **2007**, *61*, 962-970.
26
27
- 28 41. Sephton, S. M.; Dennler, P.; Leutwiler, D. S.; Mu, L.; Wanger-Baumann, C. A.; Schibli, R.;
29
30 Krämer, S. D.; Ametamey, S. M. Synthesis, radiolabelling and in vitro and in vivo evaluation of a novel
31
32 fluorinated ABP688 derivative for the PET imaging of metabotropic glutamate receptor subtype 5. *Am*
33
34 *J Nucl Med Mol Imaging* **2012**, *2*, 14-28.
35
36
- 37 42. Slavik, R.; Grether, U.; Müller Herde, A.; Gobbi, L.; Fingerle, J.; Ullmer, C.; Krämer, S. D.;
38
39 Schibli, R.; Mu, L.; Ametamey, S. M. Discovery of a high affinity and selective pyridine analog as a
40
41 potential positron emission tomography imaging agent for cannabinoid type 2 receptor. *Journal of*
42
43 *Medicinal Chemistry* **2015**, *58*, 4266-4277.
44
45
- 46 43. Pertwee, R. G.; Howlett, A. C.; Abood, M. E.; Alexander, S. P.; Di Marzo, V.; Elphick, M. R.;
47
48 Greasley, P. J.; Hansen, H. S.; Kunos, G.; Mackie, K.; Mechoulam, R.; Ross, R. A. International union
49
50 of basic and clinical pharmacology. LXXIX. Cannabinoid receptors and their ligands: beyond CB(1)
51
52 and CB(2). *Pharmacological reviews* **2010**, *62*, 588-631.
53
54
55
56
57
58
59
60

- 1
2
3 44. Paschke, A.; Neitzel, P. L.; Walther, W.; Schüürmann, G. Octanol/water partition coefficient of
4 selected herbicides: Determination using shake-flask method and reversed-phase high-performance
5 liquid chromatography. *Journal of Chemical & Engineering Data* **2004**, 49, 1639-1642.
6
7
8
9
10 45. Waring, M. J. Lipophilicity in drug discovery. *Expert opinion on drug discovery* **2010**, 5, 235-
11 248.
12
13
14
15 46. Horti, A. G.; Gao, Y.; Ravert, H. T.; Finley, P.; Valentine, H.; Wong, D. F.; Endres, C. J.;
16 Savonenko, A. V.; Dannals, R. F. Synthesis and biodistribution of [11C]A-836339, a new potential
17 radioligand for PET imaging of cannabinoid type 2 receptors (CB2). *Bioorg Med Chem* **2010**, 18, 5202-
18 5207.
19
20
21
22
23
24
25 47. Zarei, S.; Carr, K.; Reiley, L.; Diaz, K.; Guerra, O.; Altamirano, P. F.; Pagani, W.; Lodin, D.;
26 Orozco, G.; China, A. A comprehensive review of amyotrophic lateral sclerosis. *Surgical Neurology*
27 *International* **2015**, 6, 171.
28
29
30
31
32 48. Soethoudt, M.; Grether, U.; Fingerle, J.; Grim, T. W.; Fezza, F.; de Petrocellis, L.; Ullmer, C.;
33 Rothenhausler, B.; Perret, C.; van Gils, N.; Finlay, D.; MacDonald, C.; Chicca, A.; Gens, M. D.; Stuart,
34 J.; de Vries, H.; Mastrangelo, N.; Xia, L.; Alachouzos, G.; Baggelaar, M. P.; Martella, A.; Mock, E. D.;
35 Deng, H.; Heitman, L. H.; Connor, M.; Di Marzo, V.; Gertsch, J.; Lichtman, A. H.; Maccarrone, M.;
36 Pacher, P.; Glass, M.; van der Stelt, M. Cannabinoid CB2 receptor ligand profiling reveals biased
37 signalling and off-target activity. *Nature communications* **2017**, 8, 13958.
38
39
40
41
42
43
44
45
46 49. Assmus, F.; Seelig, A.; Gobbi, L.; Borroni, E.; Glaentzlin, P.; Fischer, H. Label-free assay for
47 the assessment of nonspecific binding of positron emission tomography tracer candidates. *European*
48 *journal of pharmaceutical sciences : official journal of the European Federation for Pharmaceutical*
49 *Sciences* **2015**, 79, 27-35.
50
51
52
53
54
55
56
57
58
59
60

